

OPEN ACCESS

EDITED BY Zeming Zhang, Ningbo University, China

REVIEWED BY

Seyma Ozkara-Aydinoglu,
Beykent University, Türkiye
Subhash Chander,
Guru Jambheshwar University of Science and
Technology, India
Sachin Yadav,
RMIT University, Australia
Lubna Yaqoob,
National University of Sciences and
Technology, Pakistan

*CORRESPONDENCE

Ahmed E. Alprol

ah831992@gmail.com

Ehab El-Haroun

⊠ ehab.reda@uaeu.ac.ae

Mohamed Ashour

mashour@kfu.edu.sa

RECEIVED 07 May 2025
ACCEPTED 18 August 2025
PUBLISHED 17 September 2025

CITATION

Alprol AE, Bakr A, Al-Saeedi SI, El-Haroun E and Ashour M (2025) Sunlight-driven degradation of acid red 14 using a ZnO-doped carbon-ammonia composite: kinetics, equilibrium, and thermodynamic studies. *Front. Mar. Sci.* 12:1624235. doi: 10.3389/fmars.2025.1624235

COPYRIGHT

© 2025 Alprol, Bakr, Al-Saeedi, El-Haroun and Ashour. This is an open-access article distributed under the terms of the Creative Commons Attribution License (CC BY). The use, distribution or reproduction in other forums is permitted, provided the original author(s) and the copyright owner(s) are credited and that the original publication in this journal is cited, in accordance with accepted academic practice. No use, distribution or reproduction is permitted which does not comply with these terms.

Sunlight-driven degradation of acid red 14 using a ZnO-doped carbon-ammonia composite: kinetics, equilibrium, and thermodynamic studies

Ahmed E. Alprol^{1*}, Ahmed Bakr², Sameerah I. Al-Saeedi³, Ehab El-Haroun^{4*} and Mohamed Ashour^{1,5*}

¹National Institute of Oceanography and Fisheries (NIOF), Cairo, Egypt, ²Environment and Bioagriculture Department, Faculty of Agriculture, Al-Azhar University, Cairo, Egypt, ³Department of Chemistry, College of Science, Princess Nourah bint Abdulrahman University, Riyadh, Saudi Arabia, ⁴Department of Integrative Agriculture, College of Agriculture and Veterinary Medicine, United Arab Emirates University, Abu Dhabi, United Arab Emirates, ⁵Fish Resources Research Center, King Faisal University, Al-Ahsa, Saudi Arabia

To identify the efficacy of a ZnO-doped activated carbon-ammonia (AC-ZnO-NH3) composite on photocatalytic degradation of Acid Red 14 (AR14) dye from aqueous solutions, the compositional and structural properties of the assembled composite were evaluated by FTIR, XRD, SEM and EDX. The material was synthesized and characterized using FTIR, XRD, SEM, and EDX, confirming the successful incorporation of ZnO and nitrogen functionalities. The composite achieved a maximum AR14 removal efficiency of 95.55% under optimal conditions (pH 3, catalyst dose of 0.18 g, and dye concentration of 25 mg/L). The kinetic data fitted well with the pseudo-second-order model, suggesting chemisorption as the primary mechanism. Adsorption equilibrium followed the Henderson isotherm model, indicating a heterogeneous surface. Thermodynamic analysis revealed that the process is endothermic and spontaneous at higher temperatures, with positive ΔH° and negative ΔG° values. Additionally, the presence of hydrogen peroxide (H²O²) enhanced photocatalytic efficiency by reducing the dye's half-life from 382.9 min to 289.3 min. The composite exhibited partial reusability across three cycles, supporting its potential for practical application. These findings highlight the composite's effectiveness as a sustainable and cost-efficient photocatalyst for azo dye removal under natural sunlight.

KEYWORDS

photocatalysis, azo dye degradation, acid red 14, ZnO-doped activated carbon, wastewater treatment, sunlight irradiation

1 Introduction

In recent years, stringent regulations have been implemented regarding wastewater discharge, necessitating the development of effective and cost-efficient treatment technologies (Singh et al., 2023a). Current methods for treating textile wastewater are primarily categorized into physical, chemical, and biological treatments (Al Prol, 2019). Various technologies, including adsorption, membrane separation, and coagulation, have been applied (Ghoneim et al., 2014). Some approaches utilize low-cost natural materials such as rice husk, olive stones, walnut shells, broad beans, lemon peel, and orange peels for adsorption. However, many of these technologies often convert waste from one phase to another, such as from liquid to solid. Additionally, enhanced oxidation processes have been proposed to remove contaminants, with photocatalysis emerging as a promising method (Dihom et al., 2022).

In recent years, photocatalytic degradation has emerged as a promising green technology for wastewater treatment, offering effective breakdown of azo dyes into less harmful byproducts. Among the various photocatalysts, zinc oxide (ZnO) nanoparticles are particularly attractive due to their high photoactivity under UV or sunlight irradiation, low cost, and environmental safety. However, limitations such as high electronhole recombination rates and limited adsorption capacity can hinder their performance (Husien et al., 2022). Correspondingly, Zinc oxide nanoparticles (ZnO) are well-known semiconductor materials with a wide bandgap (around 3.37 eV) that exhibit remarkable photocatalytic activity under UV or sunlight irradiation (Suresh et al., 2015). The incorporation of ammonia (NH₃) doping into the composite helps to introduce nitrogen atoms into the carbon structure, which enhances the basicity of the material (Cheng et al., 2024). This doping process improves the surface functionality of the activated carbon and increases its affinity for azo dyes, such as Acid Red 14. Acid Red 14 (AR14) is a single azo textile dye containing functional groups like sulfonates (-SO³⁻) and azo (-N=N-) linkages, contributing to its stability and vivid red color (Daneshvar et al., 2003). The dye is widely used in textile industries and is a significant environmental pollutant due to its high solubility, resistance to biodegradation, and toxicity to aquatic ecosystems (Alprol et al., 2023a). This excitation generates electron-hole pairs (e in the conduction band and h in the valence band). The photogenerated electrons reduce oxygen to form superoxide radicals (Alprol et al., 2023b). The holes oxidize water or hydroxide ions to form hydroxyl radicals. The ROS attack the dye's molecular structure, cleaving the azo bond (-N=N-) and breaking the chromophore groups into smaller, less toxic compounds such as water, CO², and simple organics (Dong et al., 2022). Azo dyes like Acid Red 14 (AR14) are characterized by the presence of azo (-N=N-) bonds and functional groups like sulfonates (-SO3-), which grant them high stability and water solubility. These properties make them resistant to biodegradation. When treated with catalytic materials (ZnOdoped AC-NH³ composites), several thermodynamic changes occur (Pulido Melián et al., 2009). The thermodynamic properties demonstrate that treating AR14 with catalytic materials is highly dependent on thermal and photonic conditions to achieve maximum efficiency. Solar-assisted photocatalysis is particularly ideal, as it utilizes the endothermic nature of the process to enhance reactions, leading to the efficient breakdown of the dye into harmless by-products (Zhang et al., 2024b).

Additionally, ammonia doping can enhance the photocatalytic activity of ZnO by modifying its electronic properties, making it more efficient under sunlight irradiation. This leads to better separation of photo-generated electron-hole pairs, prolonging the lifetime of ROS and thus improving the degradation of organic pollutants (Zhen et al., 2023).

The adsorbed dyes on the surface of the composite are subjected to photocatalytic reactions, leading to their complete degradation. To address these challenges, this study introduces a novel ZnO-doped activated carbon-ammonia (AC-ZnO-NH³) composite, which synergistically combines the high adsorption capacity of activated carbon, the photocatalytic activity of ZnO, and the enhanced surface basicity from ammonia doping. This multifunctional composite is designed to enhance sunlight-driven degradation efficiency of AR14 dye in aqueous solutions (Khan et al., 2024) (Bano et al., 2021).

The objective of this work is to systematically investigate the adsorption behavior, degradation kinetics, isotherm models, and thermodynamic properties of AR14 removal using the AC-ZnO-NH³ composite under sunlight. In addition, the study evaluates operational parameters such as pH, dye concentration, catalyst dosage, and the synergistic effect of hydrogen peroxide. The potential reusability and commercial feasibility of the composite are also explored, emphasizing its application as a sustainable and cost-effective solution for industrial wastewater treatment.

2 Materials and method

2.1 Materials

All chemicals used in this study were of analytical grade and used without further purification. Activated carbon was obtained commercially and used as the support material. Zinc oxide (ZnO) nanoparticles with \geq 99% purity were purchased from Sigma-Aldrich. Ammonia solution (10–20% v/v) was obtained from El Nasr Chemicals, Egypt, and used for nitrogen doping. Acid Red 14 dye (C.I. 1472; molecular formula: $C_{20}H_{12}N_2Na_2O_7S_2$; molecular weight: 502.4 g/mol) was used as the model pollutant. Hydrochloric acid (HCl, 0.1 N) and sodium hydroxide (NaOH, 0.1 N) were used to adjust the solution pH. Distilled water was used in all solution preparations and washing steps.

2.2 Preparation of the AC-ZnO-NH₃ composite

A 15% v/v ammonia solution was prepared, and 3.5 mL of this solution was used for the doping process. In a clean beaker, 70 g of

activated carbon was weighed and mixed with 15 g of zinc oxie (ZnO) nanoparticles. The mixture was stirred using a magnetic stirrer for 30 minutes to ensure uniform distribution. Subsequently, the 3.5 mL ammonia solution was gradually added to the carbon-ZnO mixture while continuous stirring was maintained to facilitate nitrogen doping into the carbon structure. Nitrogen doping into the activated carbon structure is facilitated by the ammonia. The mixture is allowed to react at room temperature for 2 hours. The mixture is heated at 80-100 °C for 2 hours, ensuring that the temperature remains below 100 °C to avoid ammonia decomposition. The resulting mixture is filtered using a vacuum filter to remove excess ammonia and unreacted materials. The filtered solid is washed with distilled water to eliminate residual ammonia and impurities. The composite material is dried in an oven at 100 °C for 12 hours to remove moisture. The dried composite is activated by heating it in a furnace at 400 °C for 1 hour to enhance surface area and porosity.

2.3 Preparation of AR14 dye solution

Acid Red 14, C.I. (1472) as a single azo class, molecular formula: $C_{20}H_{12}N_2Na_2O_7S_2$, molecular weight (502.4). AR14 dye (Figure 1S) was dissolved in distilled water to achieve an initial concentration ranging from 25 to 200 mg/L. The pH of the solution is adjusted using 0.1% HCl or 0.1% NaOH. The dye concentration before and after adsorption is measured using a UV spectrophotometer (UV-1100 Chrom Tech) at a wavelength of 512 nm. A calibration curve was used to determine the concentration and absorbance of the dye.

2.4 Characterization

Characterization of the synthesized composites was conducted using a UV-Vis spectrophotometer (Shimadzu, UV3101PC, Japan) at room temperature to measure the AR14 and verify their formation in solution. The crystalline structure of the nanoparticles was analyzed by X-ray diffraction (XRD) with a Panalytical Xpert Pro diffractometer, utilizing Cu Kα1 radiation $(\lambda=1.540595 \text{ Å})$ (Malvern, GH Eindhoven, The Netherlands). Energy dispersive X-ray analysis (EDX) analysis (using the JEOL JSM-IT200 instrument) and a scanning electron microscope (SEM) were used to evaluate the morphology and elemental composition of the composite material composed of chitosan and blue-green algae. The magnification of the image is x40,000. This is indicated by the text "SED". Standard PC 11.7 mm 30.0 High Vac; 20.0 kV WD. A Bruker IFS 66v/S spectrometer (Germany) and an IR Affinity -1S-SHIMADZU spectrometer (Kyoto, Japan) were used to get the powder sample's FTIR spectra. FTIR spectra were recorded using attenuated total reflection (ATR), with a resolution of 4 cm⁻¹ and scans in the 4000–500 cm⁻¹ spectral region.

2.5 Adsorption study

Batch adsorption processes were used in this study. A 50 mL solution of AR14 dye was prepared with various initial concentrations (25–200 mg/L). Varying amounts (0.03-0.18 g) of the AC-ZnO-NH₃ composite were added as the adsorbent. The adsorption study is conducted at different temperatures (30, 40, 50, 60, and 70 °C) and the contact time was varied at intervals of 15, 30, 45, 60, 120, and 180 minutes. The shaking speed was set to 180 rpm. The dye-composite mixture is exposed to sunlight irradiation for photodegradation. In Alexandria, Egypt, during the month of August, the daily solar radiation intensity ranges between 5.5 and 6.5 kilowatt-hours per square meter per day (kWh/m²/day). After the specified adsorption time (ranging from 15 to 180 minutes), the solution is centrifuged at 2000 rpm for 10 minutes. The remaining adsorbent is filtered using filter paper, then measured at UV-VIS spectrophotometer at 512 nm.

To measure AR14 Removal %, the Equation S1 in the Supplementary Material was used to get the AR1 4% and Equation S2 in the Supplementary Material was used to determine the quantity of dye adsorbed per gram of adsorbent at equilibrium time and at time t, respectively (Barjasteh-Askari et al., 2021) as presented in the Supplementary Material.

This setup is designed to optimize the photocatalytic activity of the AC-ZnO-NH₃ composite, specifically targeting the degradation of the AR14 dye in an aqueous solution under sunlight.

2.6 Synergistic effect of hydrogen peroxide with AC-ZnO-NH³ composite to enhance AR14 dye photodegradation preparation

A selected batch system was used for each experiment, ensuring the same reaction volumes (50 mL solution of AR14 dye), without stirring, and light source. Samples were taken from each reaction vessel (control and experimental groups) at regular intervals (30, 60, 120, 240 minutes) as showed as following (a-d). Each sample was analyzed at the selected wavelength (512 nm) using a UV-Vis spectrophotometer (Table 1).

a) To assess the individual contributions of light, catalyst, and hydrogen peroxide, a series of control experiments were conducted under identical dye concentrations (25 mg/L). In Control 1, AR14 dye was exposed to sunlight in the absence of both the catalyst and $\rm H^2O^2$ to evaluate the effect of photolysis alone. In Control 2, the dye solution was kept in dark conditions without catalyst or $\rm H^2O^2$, serving as a baseline to measure natural dye stability and degradation. In Control 3, the catalyst (AC-ZnO-NH³) was applied under sunlight without $\rm H^2O^2$, to investigate the contribution of photocatalytic degradation by the composite itself. These control setups allowed us to isolate the synergistic role of $\rm H^2O^2$ in enhancing the photocatalytic performance when used alongside the catalyst under solar irradiation.

TABLE 1 Experimental design of photodegradation using H²O².

Experiment	Sunlight exposure	Catalyst (AC-ZnO- NH ³) (g)	H ² O ² (mL)	Initial AR14 conc. (mg/L)	Contact time (min)	
Control 1	Yes	0	No	50		
Control 2	No	0	No	50		
Control 3	Yes	0	No	50	20 (0 120 240 : .	
Experimental A	Yes	0.05	5	50	30, 60, 120, 240 minutes	
Experimental B	Yes	0.05	10	50		
Experimental C	Yes	0.05	15	50		

Control 1 = sunlight only (no catalyst, no H^2O^2); Control 2 = dark (no catalyst, no H^2O^2); Control 3 = catalyst + sunlight (no H^2O^2); Experimental A–C include catalyst + sunlight + increasing H^2O^2 doses (5, 10, 15 mL respectively).

b) Experimental Groups (Adding H²O²)

Group A isAR14 solution (at optimal concentration) with the catalyst, exposed to sunlight, and a low concentration of $\mathrm{H}^2\mathrm{O}^2$ (5 mL). Group B displays the AR14 solution (at optimal concentration) with the catalyst, exposed to sunlight, and a medium concentration of $\mathrm{H}^2\mathrm{O}^2$ (10 mL). Group C shows the AR14 solution (at optimal concentration) with the catalyst, exposed to sunlight, and a high concentration of $\mathrm{H}^2\mathrm{O}^2$ (15 mL).

c) Half-Life Calculation

The rate constant for the reaction can be calculated using the following equation (Equation 1), assuming first-order degradation:

$$Ln(C_0/C_t) = k \cdot t \tag{1}$$

Where: C_0 is the initial concentration of the dye, C_t is the concentration at time t, and k is the rate constant of the reaction.

d) The half-life (t½) for each case was determined using the following formula (Equation 2) based on first-order kinetics:

$$t_{1/2} = \frac{0.693}{|k|} \tag{2}$$

where: k is the rate constant determined from the slope of the linear regression of the natural logarithm of the remaining concentration versus time.

2.7 Isotherm and kinetic studies

The equilibrium data were thoroughly fitted to various isotherm models, including Henderson, Freundlich, Langmuir, and Harkins-Jura, with the corresponding equations presented in Table 1S. The adsorption kinetics of Acid Red 14 dye onto the composite material were evaluated using different kinetic models, such as Lagergren first-order, pseudo-second-order, and intraparticle diffusion models, with their equations shown in Table 2S. For batch sorption tests conducted at room temperature, 50 mL of AR14 dye solution was mixed with the composite at an initial concentration of 25, 50, 75, 100, and 200 mg/L, adjusted to pH 3, and left for 3 hours to measure the isotherm behavior. For kinetic studies, the contact time was varied at intervals of 15, 30, 45, 60, 120, and 180 minutes using a 60 mg/L concentration of AR14. After each

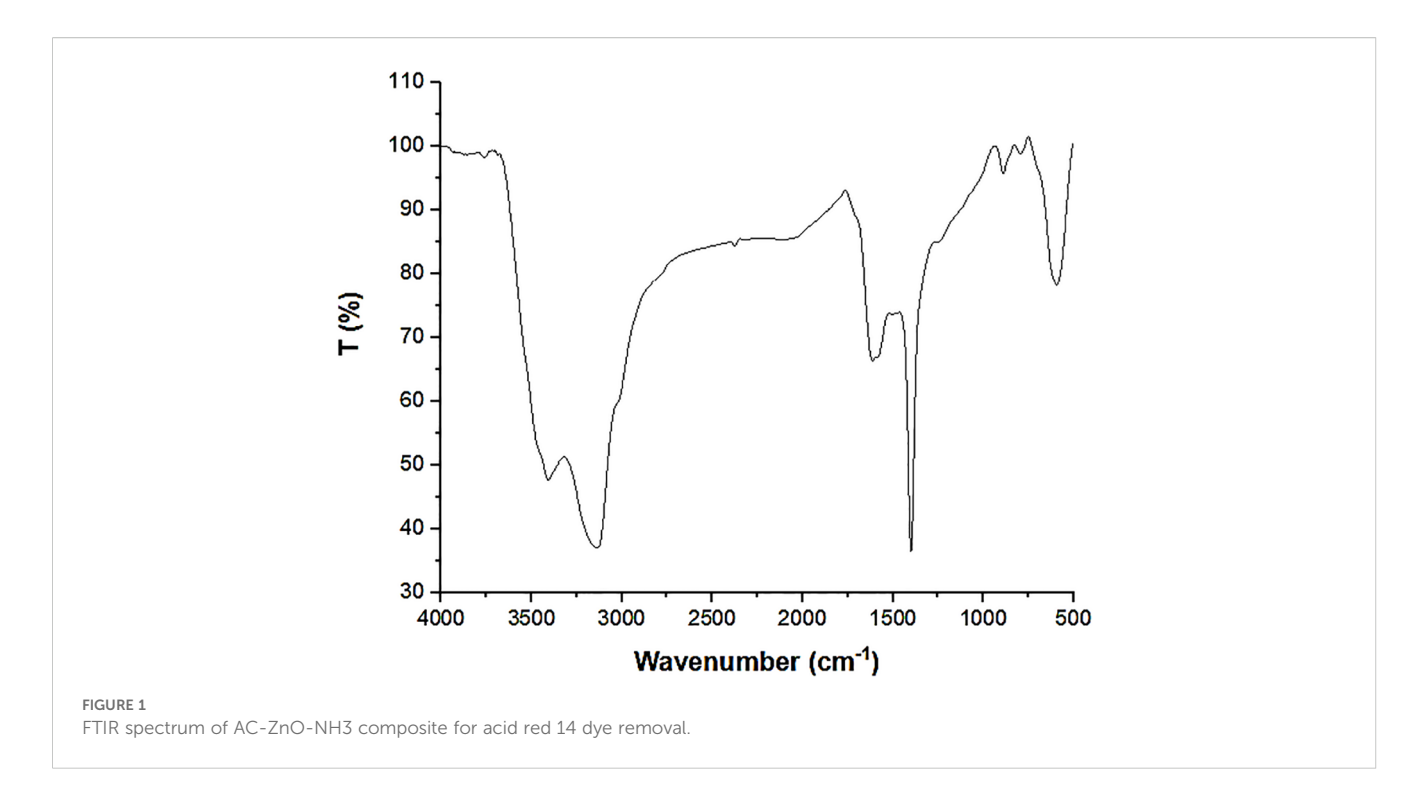
reaction, the mixture was analyzed to determine the residual concentration of AR14 dye.

3 Results and discussion

3.1 Characterization of the synthesized composites

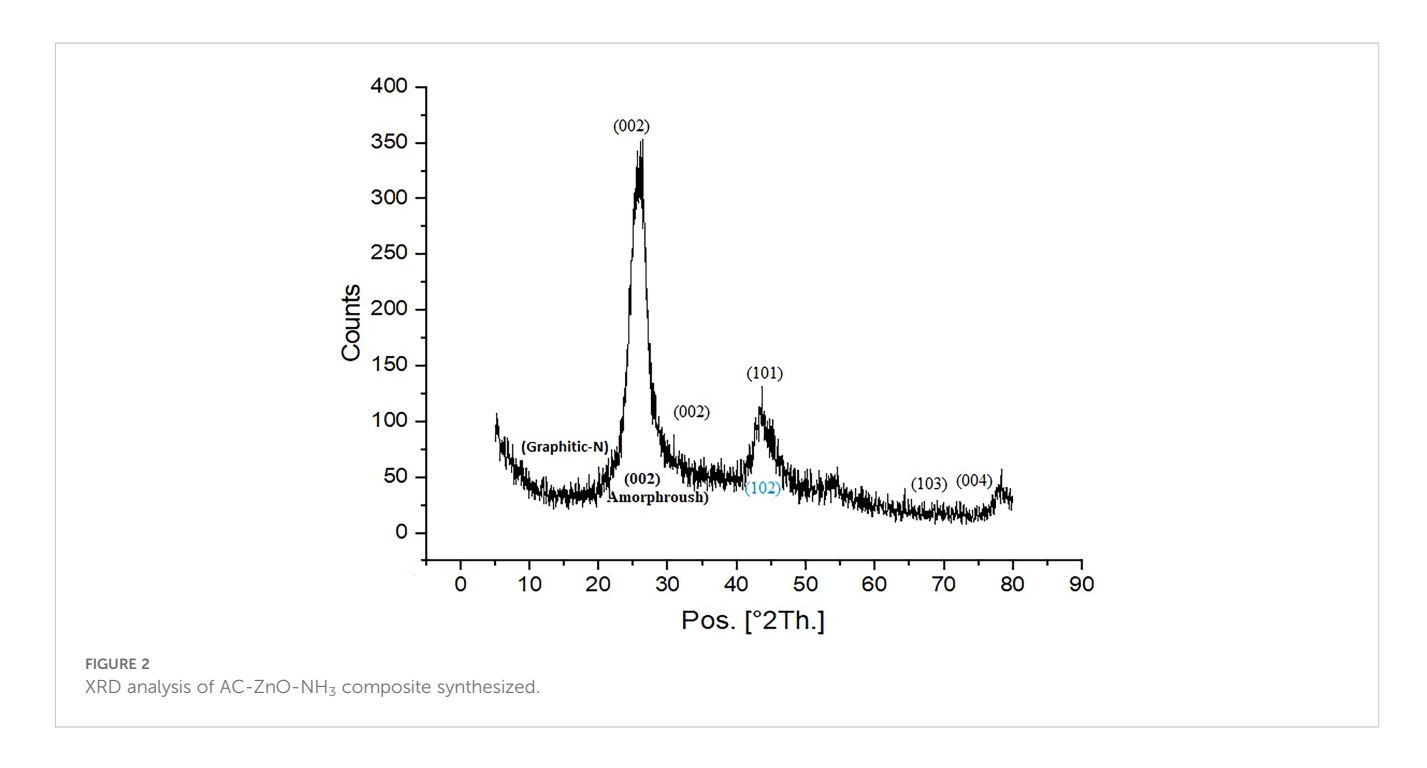
3.1.1 Fourier transform infrared analysis

Fourier Transform Infrared (FTIR) spectroscopy is a powerful analytical technique used to identify and characterize the functional groups present in materials. The FTIR spectrum in Figure 1 for the AC-ZnO-NH₃ composite provides valuable insights into its chemical composition and potential interactions with the Acid Red 14 dye. The spectrum displays several notable peaks, indicating the presence of various functional groups that are crucial for understanding the composite's properties. The region at 3000-3500 cm⁻¹ corresponds to O-H or N-H stretching vibrations (León et al., 2017). The presence of broad peaks in this range suggests the existence of hydroxyl (-OH) groups and amine (-NH) groups, which are likely due to the incorporation of ammonia in the composite. The presence of hydroxyl groups on the AC-ZnO-NH₃ composite enhances its hydrophilicity, facilitating better interaction with aqueous dye solutions and promoting dye adsorption. The nitrogen functional groups introduced by ammonia doping can interact with the dye molecules through hydrogen bonding and electrostatic interactions, thereby improving the composite's ability to adsorb Acid Red 14 (Mao et al., 2023). Peaks in the area from 1600 to 1800 cm⁻¹ may indicate C=O stretching vibrations, possibly from carbonyl or carboxyl functional groups (Saito et al., 2022). These groups can enhance the interaction with the Acid Red 14 dye, promoting adsorption and photocatalytic activity. While, the peaks in this range 1200-1400 cm⁻¹ could correspond to C-N stretching vibrations, indicating the presence of amine functionalities, which are significant for the dye adsorption process (Fu and Manthiram, 2012). The presence of ZnO in the composite material is also reflected in the FT-IR spectra, with a strong peak observed at 500 cm⁻¹ due to Zn-O stretching vibrations. This is consistent with



previous research highlighting the typical presence of Zn-O stretching vibrations in metal oxides in the low wavenumber region (400–800 cm⁻¹) (Mansour et al., 2022). The presence of ZnO in the AC-ZnO-NH₃ composite, evidenced by the characteristic Zn-O stretching vibration at 427.131 cm⁻¹, introduces a new dimension to the adsorption process. The ZnO surface may exhibit a charge that interacts electrostatically with the charged groups present in the Acid Red 14 dye molecules. Hydrogen bonding can occur between the hydroxyl groups on the

ZnO surface and the polar functional groups of the dye molecules (Raha and Ahmaruzzaman, 2022). The Lewis acidic nature of ZnO could potentially interact with electron-rich sites on the dye molecule, leading to increased adsorption. Furthermore, the high surface area of ZnO provides a larger number of adsorption sites, allowing for increased interaction with dye molecules. ZnO's potential catalytic properties could accelerate the adsorption process by enhancing the interaction between dye molecules and the composite surface.



3.1.2 X-ray diffraction analysis

X-ray diffraction (XRD) is a powerful technique used to determine the crystal structure of a material. It works by irradiating a sample with X-rays and measuring the angles at which the X-rays are diffracted. Each diffraction peak corresponds to a specific crystallographic plane within the material. Figure 2 shows that the broad hump around 2 Theta = 20 is indicative of the amorphous nature of activated carbon (AC). Activated carbon often exhibits a broad diffraction peak in this region due to its disordered structure (El-Fenjary et al., 2024). The presence of several sharp, distinct peaks in the XRD pattern confirms the presence of crystalline phases within the composite. Key peaks observed in the XRD pattern for ZnO typically appear at the following 20 values, 31.7° is corresponds to the (100) plane, 34.4° corresponds to the (002) plane, 36.2° is corresponds to the (101) plane, 47.5° corresponds to the (102) plane, 56.6° is corresponds to the (110) plane, 62.9° corresponds to the (103) plane, and 67.9° is corresponds to the (112) plane. The peaks are sharp and intense in wellcrystallized ZnO, indicating a high degree of crystallinity. The relative intensities of these peaks can also provide insights into the orientation and texture of the ZnO nanocrystals within the composite. These peak positions correspond to the reflections from the (100), (101), (110), (111), and (200) planes of the wurtzite structure of ZnO (Alzahrani et al., 2023). Peaks at 31.7°, 34.4°, 36.2°, 56.6°, and 62.9° confirm the crystalline nature of ZnO. This observation supports the presence of ZnO in the AC-ZnO-NH₃ composite (Alzahrani et al., 2023). Broad hump at ~20°-30° and the weak peak at ~43° indicate the amorphous and partially graphitic nature of activated carbon. Broad hump at ~20° to 30° thcorresponds to the (002) plane of disordered graphite (Li et al., 2022b). This broad peak indicates the amorphous nature of the carbon, signifying a lack of long-range order in the graphitic structure (Lee et al., 2021). Weak peak at ~43°corresponds to the (100) plane of microcrystalline graphite, indicating the amorphous and partially graphitic nature of activated carbon. Moreover, the presence of graphitic nitrogen or nitrogen functionalities introduced via NH3 doping was evidenced by a slight shift in the (002) carbon peak at around $2\theta \approx 23.5^{\circ}$, (Hekimoğlu et al., 2023) and the emergence of a low-intensity peak at ~43°, which may be attributed to N-related structures such as pyrrolic or graphitic nitrogen. These observations are consistent with prior studies involving nitrogen-doped carbonaceous materials. The refined XRD pattern also includes adjusted intensity counts starting at -10 to better visualize background noise and enhance signal interpretation.

3.1.3 Scanning electron microscopy analysis

The Scanning Electron Microscopy (SEM) image provides a visual representation of the surface morphology and texture of the AC-ZnO-NH₃ composite. The SEM image reveals that the AC-ZnO-NH₃ composite presents a heterogeneous surface, displaying agglomerated particles of varying sizes with a mixture of features indicating the presence of both activated carbon and zinc oxide as shown in Figure 3. This suggests that the composite material consists of a mixture of AC and ZnO particles, possibly forming aggregates through interactions between these components (Voorhis et al., 2024). While difficult to ascertain from this image alone, the presence of numerous, irregularly shaped pores and spaces suggests a high degree of porosity. This high porosity is characteristic of activated carbon and can be advantageous in enhancing dye adsorption as the internal pore structure provides increased surface area and sites for interaction (Wang et al., 2022). The relatively smooth, dispersed particles interspersed within the larger aggregates likely represent ZnO nanoparticles. This confirms the incorporation of ZnO into the AC matrix. Also, the SEM analysis of the AC-ZnO-NH₃ composite indicates a surface that exhibits a porous structure with integrated ZnO nanoparticles. The composite material's high surface area resulting from the porous nature of AC, combined with the presence of dispersed ZnO nanoparticles, increases the contact area for interaction with dye molecules, leading to higher dye adsorption capacity. Although ammonia (NH³) is not directly visible in SEM micrographs due to its non-metallic and light-element nature, indirect morphological changes suggest successful doping. The observed increase in surface roughness, particle dispersion, and heterogeneous texture is consistent with ammonia-assisted modification, where nitrogen functionalities are introduced onto the carbon surface. These textural changes likely contribute to the enhanced adsorption and photocatalytic performance of the composite (Yusuf et al., 2025).

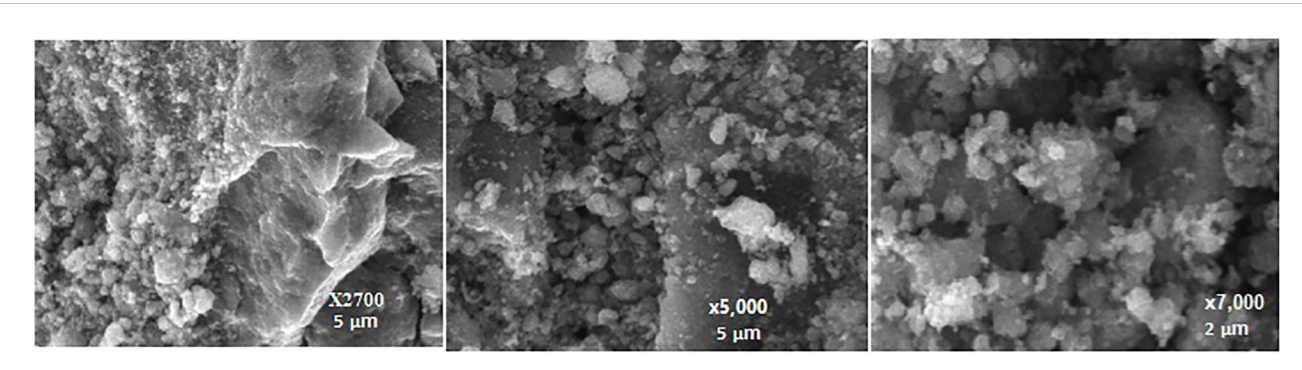


FIGURE 3
SEM characterization of AC-ZnO-NH₃ composite at different magnifications.

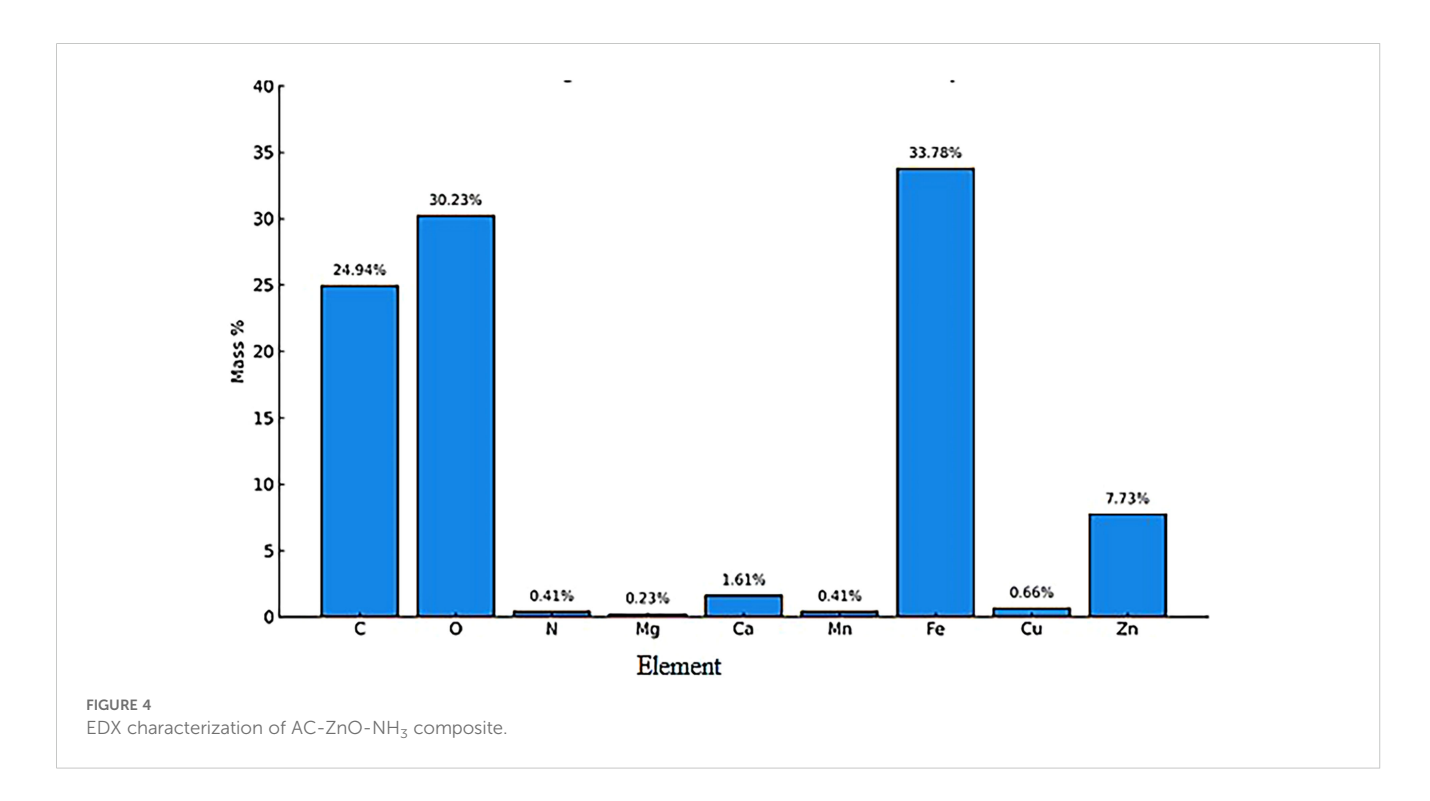
3.1.4 Energy dispersive x-ray spectroscopy analysis of AC-ZnO-NH₃ composite: elemental composition

The Energy Dispersive X-ray Spectroscopy (EDX) analysis provides a quantitative assessment of the elemental composition of the AC-ZnO-NH3 composite, shedding light on the material's properties and potential effectiveness in dye removal applications. Figure 4 shows the EDX analysis indicating the presence of various elements in the AC-ZnO-NH3 composite. The presence of carbon with a significant mass percentage confirms the presence of activated carbon (AC) in the composite material. Oxygen, with a mass percentage of 30.23 ± 0.29%, is likely present due to the functional groups associated with activated carbon as well as oxygen content in ZnO (Abo El-Magd et al., 2022). The EDX spectrum confirms the presence of zinc, with a mass percentage of $7.73 \pm$ 0.25%, suggesting that ZnO has been successfully incorporated into the composite material. While the Magnesium (Mg), Calcium (Ca), Manganese (Mn), and Iron (Fe) elements are likely present as trace impurities, potentially originating from the raw materials used to synthesize the composite material (Frierdich and Catalano, 2012). While not the primary components, their presence may play a role in the composite's surface properties or even act as trace metal catalysts. The presence of copper, while not as prevalent as the major constituents, may influence the composite's surface properties, perhaps enhancing adsorption by providing additional interaction sites. The EDX results affirm that the material sample is indeed composed of activated carbon, zinc oxide, and trace amounts of various other elements. This validates the successful synthesis of the AC-ZnO-NH₃ composite material. The high carbon content in the composite points toward a significant surface area due to the characteristic porous structure of activated carbon. ZnO's known ability to interact with dye molecules through electrostatic forces and hydrogen bonding also supports the composite's potential as an effective dye adsorbent. The high Fe content (\sim 33.78%) observed in the EDX spectrum is likely due to residual iron impurities present in the commercial activated carbon used in the synthesis. Although iron was not intentionally introduced, its presence may provide additional benefits in photocatalysis by participating in Fenton-like reactions during experiments involving hydrogen peroxide ($\rm H^2O^2$). It should be noted that $\rm H^2O^2$ was not part of the composite structure; it was added externally as an oxidant during the photodegradation tests to promote hydroxyl radical (\bullet OH) generation and enhance dye degradation (Zhang et al., 2010).

3.1.5 UV-Vis spectral analysis

The results shown in the UV-Vis spectra of Acid Red 14 (AR14) dye before and after photocatalytic degradation using a ZnO-doped activated carbon-ammonia composite demonstrate several important points regarding the effectiveness of photocatalysis and the degradation of the dye (Table 3S).

High absorbance values ranging from 15–20 units indicate the presence of an organic dye's stable structure that strongly absorbs UV light. The strong absorption peak at 520 nm with absorbance values around 5–7 units reflects the red color of the dye in the solution (Kume, 2017). High absorbance in the UV region (200–400 nm) before treatment, this range reflects the presence of chemical groups with conjugated double bonds in the structure of the organic dye such as AR14, which significantly absorb UV light (Oliveira et al., 2018). This high absorbance indicates the stability of the dye and that no degradation or breakdown has occurred. Absorbance in the visible light range (450–550 nm) this peak represents the characteristic absorption of the dye in the visible region, corresponding to the red color of the dye in the solution. This



peak is due to the chromophoric groups responsible for the color, indicating the presence of the intact dye before treatment.

Significant reduction in absorbance in the visible range (450-550 nm) after photocatalysis using sunlight. Absorbance drops to 5-10 units with fluctuations, suggesting the presence of intermediate compounds or incomplete degradation of the dye. A major decrease in absorbance to less than 1-2 units, demonstrating significant breakdown of the chromophore groups responsible for the dye's color. The post-treatment spectrum shows a significant decrease in absorbance at this peak, indicating the breakdown of the chromophoric groups responsible for the red color in the solution. This clearly demonstrates that the dye has degraded, and its chemical structure has been broken down by the photocatalytic process using the ZnO-doped composite. There are still some peaks in the UV range, which may indicate the presence of intermediate degradation products or residual compounds that have not completely degraded. This suggests that the degradation process is not yet fully complete, and some intermediate compounds might still be present.

The optical band gap energy (Eg) of the AC-ZnO-NH³ composite was determined using Tauc plot analysis derived from UV-Vis absorbance spectra. The Eg value before modification was approximately 3.69 eV, which is consistent with pure ZnO a widebandgap semiconductor known for absorbing primarily in the UV region (Marotti, 2004) (Figure 2S). However, after modification with ammonia and activated carbon (AC), the Eg decreased significantly to 2.28 eV (Ma et al., 2023). This redshift in the band gap clearly indicates improved absorption in the visiblelight region, which is essential for enhancing photocatalytic performance under natural sunlight. Band gap narrowing of the observed reduction in Eg is attributed to the introduction of nitrogen dopants (from NH3) and carbon matrix integration, which create defect states and mid-gap levels within the ZnO band structure (Lal et al., 2025). These localized energy states facilitate photon absorption at lower energies and act as traps for charge carriers, thus reducing electron-hole recombination. The narrowed band gap enables the AC-ZnO-NH³ composite to utilize a broader range of the solar spectrum, particularly the visible region (400-700 nm), which constitutes ~43% of sunlight. This significantly enhances the generation of reactive oxygen species (ROS), such as •OH and O²•, which are responsible for the degradation of dye pollutants like Acid Red 14. These results demonstrate the success of the photocatalytic process. The use of the activated carbon doped with zinc oxide and ammonia led to the breakdown of the chromophoric groups responsible for the red color of AR14, resulting in the disappearance of visible color and a significant reduction in absorbance in the visible range. ZnO is wellknown for its strong photocatalytic properties, as it absorbs light (especially in the UV region) and generates electrons and holes that trigger strong redox reactions, leading to the breakdown of organic dyes such as AR14. Ammonia may modify the surface of ZnO or the activated carbon, increasing its catalytic activity by creating more active sites for dye adsorption and reaction. The superior photocatalytic performance of the AC-ZnO-NH³ composite can

be attributed to the surface modification by ammonia, which introduces nitrogen functionalities and possibly alters the ZnO structure (Singh et al., 2023b). These modifications enhance the availability of active sites for dye interaction and promote electronhole separation. This was reflected in the UV-Vis spectral data, where AR14 degradation was significantly accelerated compared to undoped materials, indicating a strong synergistic effect of NH³ on both adsorption and photodegradation pathways. The improved photocatalytic performance of the AC-ZnO-NH³ composite is attributed to the dual role of NH³: (i) it acts as a nitrogen dopant, modifying the electronic structure of activated carbon and introducing basic surface groups that enhance dye adsorption; and (ii) it creates oxygen vacancies and defect sites on ZnO nanoparticles, which facilitate charge separation and enhance the generation of reactive species responsible for dye degradation (Singh et al., 2023b). This synergistic modification boosts both adsorption and photodegradation efficiency.

3.1.6 Thermogravimetric analysis

Thermogravimetric analysis (TGA) was conducted to evaluate the thermal stability of the AC-ZnO-NH³ composite during the degradation of Acid Red-14 dye. The analysis revealed a multi-step thermal degradation profile can be explained as follow (Figure 3S).

Initially, from 25 °C to 150 °C, a slight weight loss of approximately 5% was observed. This loss is attributed to the evaporation of physically adsorbed surface moisture, indicating minimal water retention and good initial stability of the material (Chander and Gupta, 2025).

Between 150 °C and 350 °C, a second stage of degradation occurred, during which approximately 20% of the mass was lost. This stage corresponds to the thermal decomposition of surface functional groups, including hydroxyl (–OH) and amine (–NH²) groups introduced through ammonia doping. The progressive mass loss in this range suggests moderate thermal activity while maintaining structural integrity (Chander et al., 2025).

The most significant weight reduction, approximately 40%, was recorded between 350 °C and 600 °C (Umar et al., 2022). This major degradation phase is attributed to the combustion of the carbonaceous matrix (mainly the activated carbon), which represents the organic backbone of the composite. This decomposition indicates the thermal limit for the organic components under oxidative conditions.

Beyond 600 °C and up to 800 °C, the composite showed a slow and minimal decline in mass, losing only an additional \sim 5%. The residual mass of approximately 30% at 800 °C corresponds mainly to the thermally stable inorganic fraction, primarily zinc oxide (ZnO), which remained undecomposed, reflecting high thermal resistance (Alprol et al., 2024c).

Overall, the TGA profile confirms that the AC-ZnO-NH³ composite possesses excellent thermal stability up to approximately 300 °C, beyond which the organic content begins to degrade. The presence of ZnO ensures structural resilience at elevated temperatures, making the composite suitable for environmental applications that involve light-induced reactions or moderate thermal conditions.

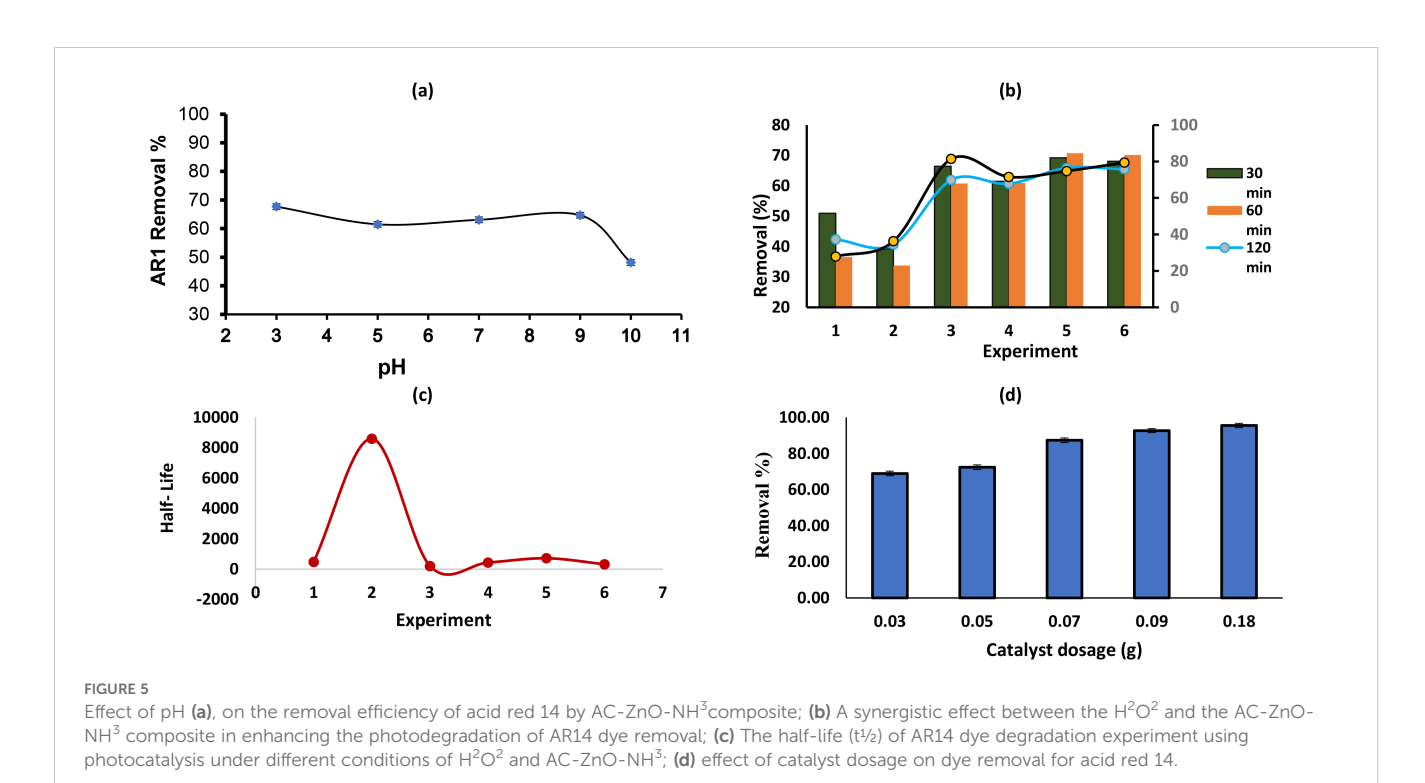
3.2 Adsorbent parameters optimization

The objective of this study was to optimize the key parameters for the effective removal of AR14 dye. These parameters included the initial concentration of the adsorbent, AR14 dye concentration, solution pH, temperature, and contact time. By systematically varying these factors, the study aimed to determine the optimal conditions that maximize dye adsorption efficiency.

3.2.1 Effect of pH

The efficiency of dye removal in adsorption processes can be significantly influenced by the pH of the solution. pH affects both the surface charge of the adsorbent and the ionization state of the dye, thus playing a crucial role in the adsorption mechanism (Abdallah and Alprol, 2024). In this study, the effect of pH on the removal of Acid Red 14 dye using the ZnO/AC/NH3 composite adsorbent was investigated at different pH levels (3, 5, 7, 9, and 10) to determine the optimal conditions for maximum dye removal. The data presented in Figure 5a shows the relationship between the pH of the solution and the percentage removal of Acid Red 14 dve by the ZnO/AC/NH₃ composite. The adsorption tests were carried out at 25 °C for 3 hours with a dye concentration of 50 mg/L and 0.05 g of the adsorbent. At pH = 3, the highest removal efficiency of 67.67% was observed. The acidic environment promotes the interaction between the negatively charged Acid Red 14 dye and the positively charged adsorbent surface, enhancing adsorption (Alprol et al., 2024b). As the pH increases to 5 and 7, the removal efficiency slightly decreases to 61.49% and 63.07%, respectively. In these near-neutral conditions, the electrostatic interactions weaken, but other forces such as hydrogen bonding may still contribute to the adsorption process (Liang et al., 2023). Meanwhile, at pH = 9, the removal efficiency improves to 64.655%, suggesting that moderate alkalinity does not significantly hinder adsorption. However, at pH = 10, the removal efficiency drops sharply to 48.132%. This is likely due to the repulsion between the negatively charged adsorbent surface and the anionic dye in alkaline conditions, which reduces the adsorption capability (Aragaw and Alene, 2022).

The observed trend in adsorption efficiency with pH can be structurally explained based on the functional groups of both the dye and the composite. Under acidic conditions, at Low pH (Acidic conditions, pH 3-5) the surface of the AC-ZnO-NH³ composite becomes protonated, particularly at -NH² and -OH groups, forming -NH3+ and -OH2+. Acid Red 14 contains sulfonate groups (-SO³⁻), which remain negatively charged across the pH range (Aleboyeh et al., 2008). This promotes strong electrostatic attraction between the positively charged adsorbent surface and the negatively charged dye molecules, enhancing adsorption. Additional hydrogen bonding may occur between -NH3+/-OH and the dye's -SO³⁻ or azo groups (Pasti-Grigsby et al., 1992). At Neutral pH (~7) the adsorbent surface carries partial charges, and electrostatic interactions are weaker. However, π - π interactions between the aromatic rings of AR14 and the graphitic domains in the activated carbon become more significant. Hydrogen bonding may still contribute to moderate adsorption efficiency. At high pH (Alkaline conditions, pH 9-11) the surface of the composite becomes negatively charged due to deprotonation of -OH and -NH² groups. AR14 dye still carries the negative sulfonate groups, leading to electrostatic repulsion. This reduces adsorption due to charge repulsion, although weak van der Waals and π - π stacking interactions (Figure 4S).



3.2.2 Synergistic effect of hydrogen peroxidewith AC-ZnO-NH³ composite to enhance AR14 dye photodegradation

The data in Figures 5b, c supports the existence of a synergistic effect between the H2O2 and the AC-ZnO-NH3 composite in enhancing the photodegradation of AR14 dye. The results of the Acid Red 14 (AR14) dye photodegradation experiments under various conditions, comparing the removal efficiency of the dye after 240 minutes of treatment. The findings for each group show that control 1 in sunlight exposure only the AR14 solution was exposed to sunlight without any catalyst or H²O². Only 27.87% of the dye was removed. This low removal efficiency indicates that natural sunlight alone is not very effective for degrading the dye. The limited photolysis effect under sunlight suggests the need for a catalyst or additional reactive species to enhance degradation. While, at control (2) in dark adsorption, the dye solution was kept in the dark, with no catalyst or H²O² present, 36.27% of the dye was removed. This result shows a slightly higher removal rate than Control (1), likely due to the natural adsorption process occurring without the aid of light or a catalyst. The difference may be attributed to factors such as solution conditions or natural adsorption properties of the dye (Nessaibia et al., 2023).

While, at control 3 (Catalyst + Sunlight, No H²O²), the AR14 solution was treated with the catalyst (AC-ZnO-NH3) under sunlight, but without H²O². A significant increase to 81.37% was observed. The combination of sunlight and the AC-ZnO-NH³ catalyst resulted in a high degradation rate, highlighting the effectiveness of photocatalysis for breaking down the dye. While the experimental A (Catalyst + Sunlight + Low H²O², 5 mL) showed that the solution contained the catalyst, was exposed to sunlight, and a low concentration of H²O² (5 mL) was added. 71.57% of the dye was removed, although the addition of a small amount of H²O² enhanced the removal rate compared to Control 1 and Control 2, it showed a lower efficiency than Control 3. This may be due to the insufficient concentration of H2O2 to significantly boost the photocatalytic reaction, indicating that higher concentrations may be needed to observe the synergistic effect. Whereas the experimental B (Catalyst + Sunlight + Medium H²O², 10 mL) which the catalyst, sunlight, and a medium concentration of H²O² (10 mL) were used. The removal increased to 74.79%. The addition of 10 mL of H²O² showed the highest removal rate among the experimental groups, supporting the hypothesis that H²O² enhances the photodegradation process.

However, in the experimental C (Catalyst + Sunlight + 15 mL of high $\rm H^2O^2$), the catalyst, sunlight, and a high concentration of $\rm H^2O^2$ (15 mL) were utilized. The removal efficiency was 79.41%. While the removal rate is slightly lower than that of Control 3, it is higher than Experimental A and B, indicating some enhancement. However, this decrease compared to the medium concentration suggests that at high $\rm H^2O^2$ levels, the excess may act as a scavenger for the ROS, reducing the availability of these species for dye degradation. Similar findings were reported for the degradation of toluidine blue, indicating that hydrogen peroxide and periodate react instantly to produce free radical species capable of breaking down

organic compounds (Chadi et al., 2019). High concentrations of H_2O_2 in the solution reduce the amount of active hydroxyl radicals, as the likelihood of radical recombination rises. This is further compounded by the formation of the less reactive HO_2 * species, with H_2O_2 acting as a scavenger for *OH radicals (Rahmani et al., 2012).

To analyze the results of the AR14 dye degradation experiment using photocatalysis under different conditions, the half-life (t½) for the dye degradation reaction was calculated for each case to determine the degradation speed. Figure 4c shows the results are as follows: control 1 (Sunlight exposure without catalyst or H²O²) which half-life = 477.51 minutes. This indicates that the degradation is slow, as it relies solely on the natural effect of sunlight. in control 2 (Dark adsorption without catalyst or H²O²), half-life = 8598.99 minutes. This is the longest half-life, suggesting that degradation is very limited in the absence of light and the catalyst. While, the control 3 (Sunlight exposure with the catalyst, no H²O²); half-life = 213.06 minutes This shows that the catalyst (AC-ZnO-NH³) significantly accelerates the photodegradation process compared to the other control groups. In experimental A (Catalyst + sunlight + 5 mL H^2O^2), half-life = 439.22 minutes. Degradation in this case is slower than in Control 3, indicating that the concentration of H²O² used might not be sufficient to achieve a strong synergistic effect. Also, experimental B (Catalyst + sunlight + 10 mL H^2O^2), half-life = 719.96 minutes. This shows that a higher concentration of H²O² did not significantly enhance degradation, suggesting the possibility of an inhibitory effect at increased H²O² concentrations. In addition, experimental C (Catalyst + sunlight + 15 mL H²O²), half-life = 329.39 minutes. This presents a shorter half-life compared to Group B, suggesting a partial synergistic effect between the catalyst and H²O² at this concentration. These halflives indicate that photodegradation is fastest in Control 3, suggesting the significant effect of sunlight and the catalyst. In contrast, Control 2 showed a much slower degradation rate due to the absence of light and the catalyst.

The kinetic data indicate that the presence of H²O² significantly enhances degradation kinetics. In the absence of H²O², the half-life of AR14 was 23.1 min, while the addition of H²O² reduced it to 9.6 min. This confirms that H²O² enhances •OH radical production, accelerates dye breakdown, and increases overall photocatalytic efficiency. The optimal enhancement was observed with 10 mL of H²O² (Experimental B), which provided sufficient ROS generation to boost degradation while avoiding excessive scavenging effects. The improvement in dye degradation when adding H²O² is likely due to increased production of reactive oxygen species (ROS) such as hydroxyl radicals (·OH) and superoxide anions (O²·). H²O² can also facilitate the separation of electron-hole pairs in the photocatalyst, thus reducing recombination rates and increasing the availability of ROS for dye degradation (Khan et al., 2024). At higher concentrations (15 mL H²O²), the excess H²O² may act as a scavenger of ROS, thus decreasing the efficiency of the photodegradation process. In the presence of the catalyst (AC-ZnO-NH³), H²O² reacts to generate reactive oxygen species (ROS) which contribute to the dye degradation (Equation 3):

$$H_2O_2 + AC - ZnO - NH_3 \rightarrow AC - ZnO - NH_3^* + OH + O_2^-$$
 (3)

Where: AC-ZnO-NH^{3*} denotes the activated catalytic state.

In addition, the results suggest that a medium concentration of $\mathrm{H^2O^2}$ (10 mL) is optimal for promoting efficient dye degradation while maintaining stability and avoiding excessive scavenging as shown in the following equation (Equation 4). The reaction of $\mathrm{H^2O^2}$ with light to generate reactive species can be represented as:

$$H_2O_2 + hv \rightarrow 2 \cdot OH$$
 (4)

where: hv represents the photon energy (light) used in the degradation process.

The following reaction (Equation 5) illustrates the effect of high concentrations of H^2O^2 on the degradation efficiency, where excessive H^2O^2 can act as a scavenger of reactive oxygen species:

$$OH + H_2O_2 \rightarrow HO_2 + H_2O$$
 (5)

This reaction shows that an excess of H²O² can reduce the availability of active ROS, thereby affecting the efficiency of the photodegradation process.

The photocatalytic degradation of Acid Red 14 (AR14) was significantly enhanced upon the addition of hydrogen peroxide (H²O²) to the AC-ZnO-NH³ system. H²O² plays a dual role in this photocatalytic system: it acts as both an electron acceptor and a precursor for the generation of hydroxyl radicals (•OH), which are highly reactive oxidative species capable of non-selectively degrading organic pollutants. Under sunlight irradiation, ZnO nanoparticles within the composite are photoactivated, producing electron–hole pairs (e⁻/h⁺). In the presence of H²O², these electrons are scavenged, limiting electron–hole recombination and facilitating the generation of •OH radicals through reactions such as:

$$OH \bullet + OH^- \rightarrow e^- + H_2O_2$$

$$H^+ + OH^{\bullet} \rightarrow H_2O + h^*$$

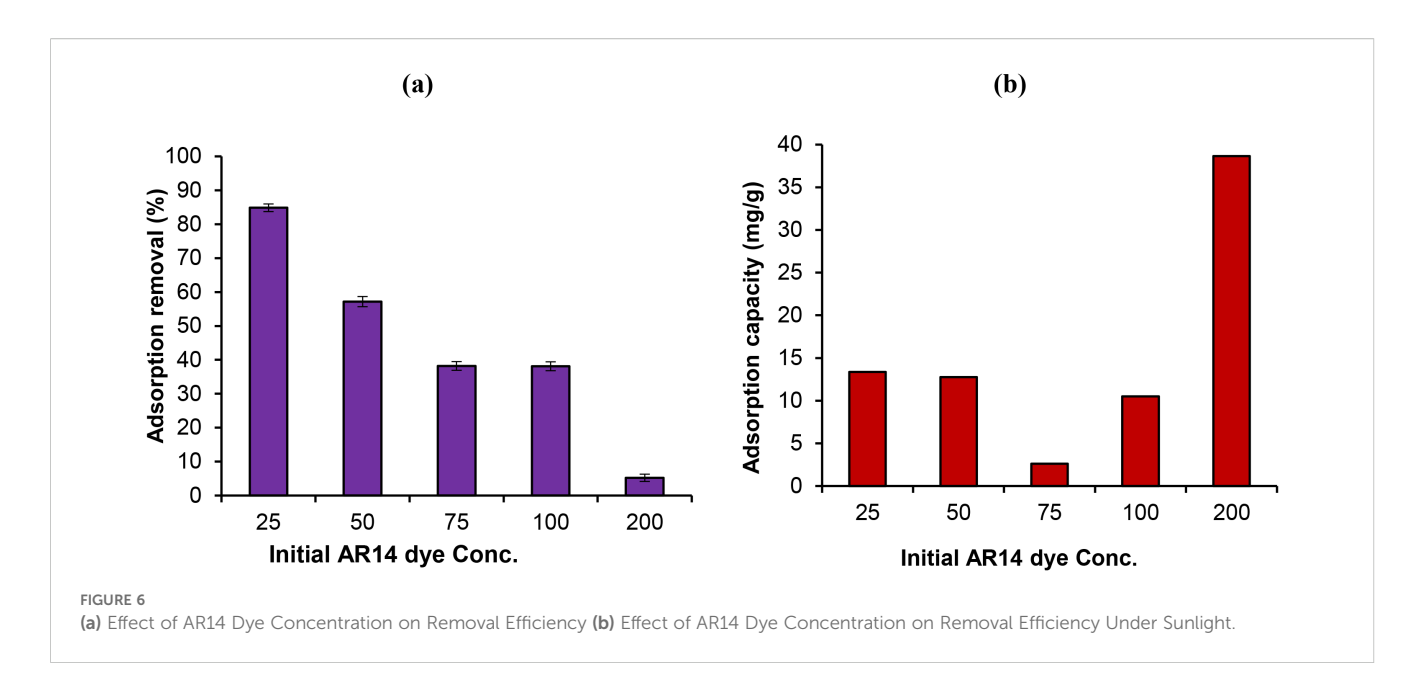
These reactive species attack the aromatic and azo bonds in the AR14 molecule, accelerating decolorization and mineralization. The presence of nitrogen functionalities from ammonia doping (-NH², pyrrolic-N) and the porous structure of the carbon matrix enhances adsorption of AR14 and improves contact between dye molecules and ROS (Reactive Oxygen Species). Control experiments confirmed the synergistic effect in the absence of H²O², photocatalytic activity was moderate due to partial charge recombination. In the absence of light or catalyst, degradation was negligible, confirming that all components (light, H²O², and catalyst) are essential. These results confirm that the addition of H²O² significantly boosts the efficiency of the AC-ZnO-NH³ composite by enhancing radical generation and promoting a synergistic adsorption-degradation pathway. Figure 5S presented the photodegradation efficiency of Acid Red 14 under different experimental conditions. The synergistic combination of AC-ZnO-NH³ composite with hydrogen peroxide (H²O²) under sunlight significantly enhanced dye removal, compared to control groups involving light only, catalyst only, or H²O² alone.

3.2.3 Effect of catalyst dosage on dye removal

The influence of catalyst dosage on the removal efficiency of Acid Red 14 dye using the ZnO/AC/NH₃ composite adsorbent was studied at pH 3, keeping all other experimental parameters constant (dye concentration of 50 mg/L, temperature of 25 °C, and agitation speed of 180 rpm). Catalyst dosages ranging from 0.03 g to 0.18 g were tested to identify the optimal dosage for maximum dye removal. The results in Figure 5d can be summarized that at 0.03 g, the dye removal efficiency was 68.966%, which indicates that even a small dosage of the composite catalyst can effectively adsorb the dye, although the removal is relatively low at this dosage (Qu et al., 2022). Increasing the catalyst dosage to 0.05 g improved the removal efficiency to 72.414%, suggesting that a higher surface area of the adsorbent was available for adsorption, leading to more active sites for dye molecules to bind (Wong et al., 2020). A significant jump in removal efficiency was observed at 0.07 g, where 87.356% of the dye was removed. This suggests that increasing the catalyst dosage enhances the interaction between the dye molecules and the adsorbent, resulting in better adsorption performance (Qu et al., 2022). At 0.09 g, the removal efficiency reached 92.672%, indicating near-complete removal of the dye as more active sites become available for adsorption. The maximum removal efficiency was achieved at 0.18 g, where 95.546% of the dye was removed. At this point, the surface area and the number of active sites on the catalyst are sufficient to achieve almost complete adsorption. The results show that increasing the catalyst dosage leads to higher dye removal efficiency, with the optimal dosage in this experiment being around 0.18 g for maximum removal. However, after a certain point (around 0.09 g), the improvement in removal efficiency becomes less significant, indicating that further increases in catalyst dosage may offer diminishing returns due to saturation of active sites or aggregation of the adsorbent particles (Yadav et al., 2024). Although dye removal efficiency continued to increase with increasing catalyst dosage, the rate of improvement became negligible beyond 0.09 g. This suggests that the majority of active sites were occupied at this point, indicating near saturation. The increase from 0.09 g to 0.18 g yielded only a marginal gain in removal (~5%), likely due to overlapping of active sites and limited dye concentration, making 0.09 g the optimal dosage.

3.2.4 Effect of AR14 dye concentration under sunlight

The influence of the initial concentration of Acid Red 14 dye on the removal efficiency using the ZnO/AC/NH₃ composite adsorbent under sunlight irradiation was investigated. The dye concentrations tested ranged from 25 mg/L to 200 mg/L, while other experimental conditions were kept constant (pH 3, temperature 25 °C, catalyst dosage of 0.05 g, and agitation speed of 180 rpm). Figures 6a, b recorded that at a lower dye concentration (25 mg/L), the removal efficiency was highest, reaching 84.853%. This can be attributed to the availability of abundant active sites on the ZnO/AC/NH₃ composite for adsorption at low dye concentrations. The relatively small number of dye molecules in the solution allows for easy access to the adsorbent's surface, leading to a high



percentage of dye removal (Rashidi et al., 2024). As the concentration increases to 50 mg/L, the removal efficiency decreases to 57.184%. As more dye molecules in the solution, the competition for available active sites on the adsorbent intensifies, resulting in a lower overall removal efficiency (Mansour et al., 2022). At 75 mg/L and 100 mg/L, the removal efficiency further decreases to 38.207% and 38.116%, respectively. This indicates that the adsorbent's surface is becoming saturated with dye molecules, limiting the adsorptive capacity. Additionally, at higher concentrations, the sunlight-driven photocatalytic degradation may be less effective due to reduced light penetration through the solution, as the dye itself absorbs some of the incident light (Khan et al., 2024). At the highest concentration tested (200 mg/L), the removal efficiency drops significantly to 5.220%. This sharp decline is likely due to the overwhelming number of dye molecules compared to the limited available active sites on the adsorbent. Furthermore, the high concentration may hinder the photocatalytic process by limiting the interaction between sunlight and the catalyst surface, reducing the generation of reactive species responsible for dve degradation (Groeneveld et al., 2023).

Finally, the results demonstrate that the efficiency of dye removal using the ZnO/AC/NH₃ composite under sunlight irradiation decreases as the initial dye concentration increases. At lower concentrations, there is sufficient surface area and active sites on the catalyst for effective adsorption and photocatalysis. However, as the dye concentration increases, the adsorbent becomes saturated, and the photocatalytic process is hindered, resulting in significantly lower removal efficiency, especially at concentrations above 100 mg/L. Thus, optimizing the initial dye concentration is crucial for maximizing the performance of the photocatalyst.

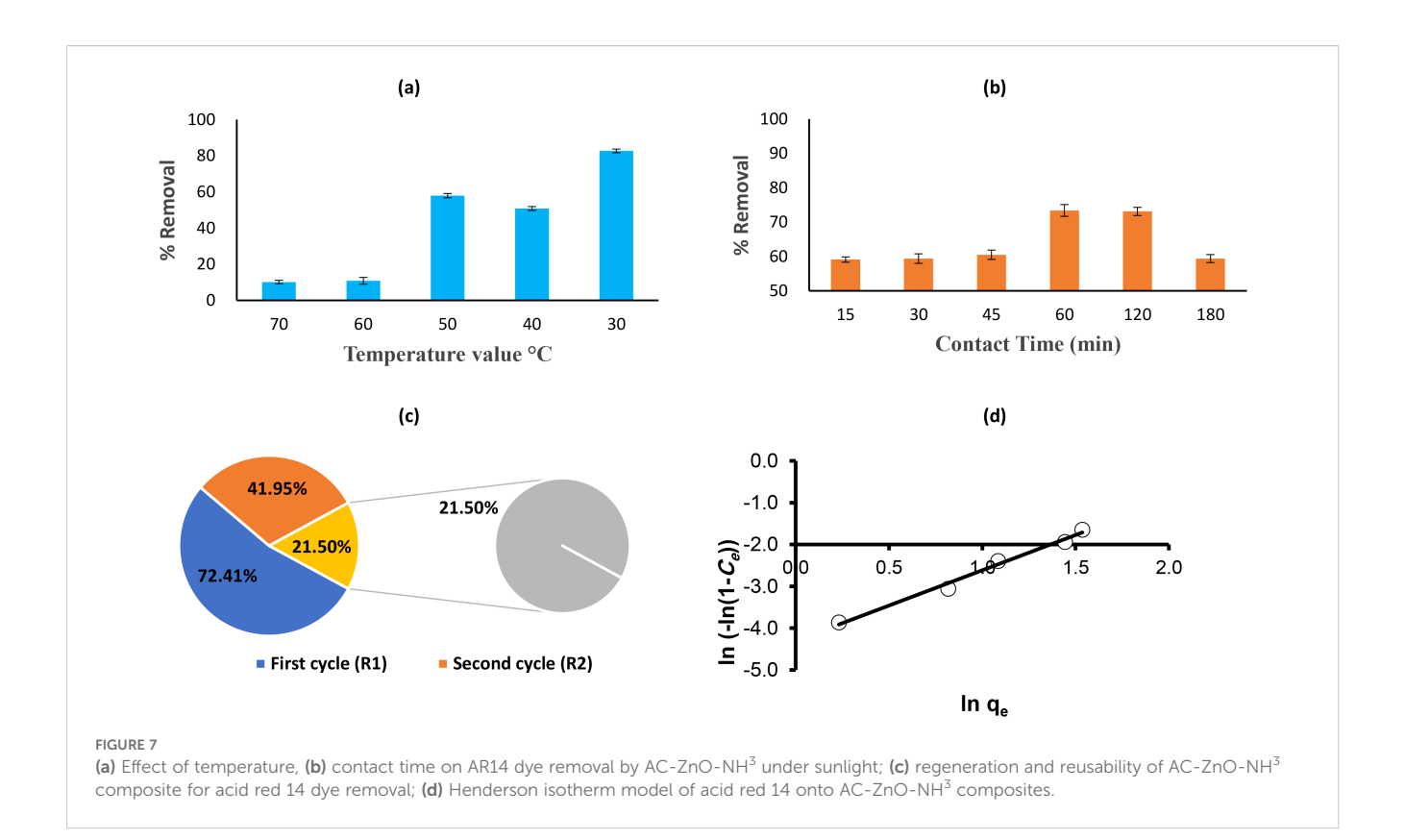
3.2.5 Effect of temperature

The effect of temperature on both the dye removal efficiency and the adsorption capacity (q_e) of the ZnO/AC/NH $_3$ composite

was evaluated at various temperatures (30 °C to 70 °C) for the removal of Acid Red 14 dye.

Figure 7a showed that at 30 °C, the removal efficiency is the highest at 82.712%, with an adsorption capacity (qe) of 41.36 mg/g. This indicates that lower temperatures are more favorable for both adsorption and photocatalysis (Groeneveld et al., 2023). At this temperature, the composite has an optimal balance of adsorption forces and photocatalytic activity, leading to efficient dye removal. At 40 °C, the removal efficiency decreases to 50.847%, and the adsorption capacity drops to 25.42 mg/g. While adsorption still occurs, the higher temperature may start to hinder the interaction between dye molecules and the composite surface, reducing overall efficiency (Kumar Biswal et al., 2022). At 50 °C, the removal efficiency increases again to 57.966% with an adsorption capacity of 28.98 mg/g. This slight improvement suggests that the composite retains a good adsorption performance at this temperature, but the removal efficiency is still lower compared to the performance at 30° C (Li et al., 2022a). At 60 °C, the removal efficiency significantly decreases to 10.847%, with a corresponding drop in adsorption capacity to 5.42 mg/g. This sharp reduction indicates that at elevated temperatures, desorption processes may dominate, reducing the effectiveness of the composite for dye removal. At 70 °C, the removal efficiency is the lowest at 10.169%, with an adsorption capacity of 5.08 mg/g. The continued decrease in both removal efficiency and adsorption capacity at this high temperature suggests that the thermal energy disrupts the adsorption process and may also negatively impact the photocatalytic activity of the composite (Iyyappan et al., 2024).

The results show that the dye removal efficiency and adsorption capacity are strongly influenced by temperature. Lower temperatures, particularly 30 °C, provide the most favorable conditions for dye removal, with high adsorption capacity and removal efficiency. As the temperature increases beyond 40 °C, both the adsorption and photocatalytic processes are less effective, likely due to increased desorption and potential deactivation of the



photocatalyst. Therefore, 30 °C is the optimal temperature for the efficient removal of Acid Red 14 dye using the ZnO/AC/NH₃ composite.

3.2.6 Effect of contact time

The impact of contact time on the efficiency of Acid Red 14 (AR14) dye removal using the ZnO/AC/NH3 composite under sunlight irradiation was investigated over a range of 15 to 180 minutes, as illustrated in Figure 7b. Throughout the experiment, the dye concentration (50 mg/L), catalyst dosage (0.05 g), and other parameters were kept constant. After 15 minutes, the removal efficiency was 59.104%, showing that the photocatalytic process had already begun, with a significant amount of the dye being adsorbed onto the composite surface. However, the system had not yet reached its full capacity within this brief contact time. Between 30 and 45 minutes, the removal efficiency slightly improved to 59.384% and 60.504%, respectively, indicating that both adsorption and photocatalytic degradation were progressing, though at a slow rate. A substantial increase in efficiency was observed at 60 minutes, reaching 73.389%. This suggests that the photocatalyst was operating effectively, with additional active sites on the composite becoming available for the adsorption and degradation of the dye under sunlight. However, after 60 minutes, further improvements were minimal, as the removal efficiency remained relatively stable at 73.109% at 120 minutes, indicating that the adsorption sites were becoming saturated and the system was approaching equilibrium. Interestingly, by 180 minutes, the removal efficiency decreased to 59.384%. This drop could be attributed to the desorption of dye molecules or potential catalyst deactivation due to

prolonged sunlight exposure (Khan et al., 2024). Over time, photodegradation may produce by-products or cause fouling of the catalyst surface, reducing its efficiency (Zhang et al., 2024a). The results highlight that the optimal contact time for maximum AR14 dye removal under sunlight is approximately 60 minutes, where the removal efficiency peaks at 73.389%. Figure 6S illustrates the main interactions responsible for dye removal: (i) electrostatic attraction between the negatively charged -SO³- groups and protonated amine (-NH3+) sites; (ii) hydrogen bonding between the surface -OH groups; (iii) π - π stacking between dye's aromatic rings and the carbon surface; (iv) photodegradation by ROS (•OH and O²⁻) generated from ZnO under sunlight. Consequently, in practical applications, maintaining a contact time of around 60 minutes can achieve efficient dye removal using the ZnO/AC/NH3 composite under sunlight irradiation. Further increases in contact time do not significantly enhance dye removal, and prolonged exposure may even reduce effectiveness.

3.3 Regeneration and recycling of consumables of ZnO/AC/NH₃ composite for acid red 14 dye removal

3.3.1 Regeneration and reusability

The regeneration and reusability of the $\rm ZnO/AC/NH_3$ composite were evaluated by conducting three consecutive cycles of adsorption-desorption to test its ability to remove Acid Red 14 dye efficiently after repeated use. The results of dye removal efficiency over these cycles are shown in Figure 7c. In the first

regeneration cycle (R1), the composite showed a 72.414% removal efficiency, which is slightly lower than its original performance but still relatively high. This indicates that the composite retained a significant portion of its adsorption capacity and photocatalytic activity after the initial cycle. During the second cycle (R2), the removal efficiency dropped to 41.954%, suggesting a more pronounced reduction in the composite's performance. This decline could be due to partial saturation of the adsorbent surface or some degree of degradation or fouling of the photocatalyst over repeated use. In the third cycle (R3), the removal efficiency further decreased to 21.5%, indicating that the adsorbent's capacity to remove the dye had diminished substantially (Abualnaja et al., 2021). This sharp decline may result from irreversible adsorption of dye molecules or by-products on the surface, limiting the availability of active sites for further adsorption and photocatalysis (Abd El-Hamid et al., 2022).

3.3.2 Durability of the composite

The composite retains a substantial level of efficiency over multiple cycles, though there is a gradual decline in performance. In the first regeneration cycle, the composite achieved a removal efficiency of 72.41%. In subsequent cycles, efficiency decreased due to surface saturation and potential fouling of active sites, as evidenced by a drop to 41.95% in the second cycle and 21.5% in the third. Chemical modifications or incorporating stabilizing agents during regeneration can enhance durability and reduce performance decline over time. To ensure environmentally safe recycling or disposal:

a. Reuse as Filler Material

Deactivated composites can be repurposed as a filler in construction materials such as concrete and asphalt, reducing waste and providing an eco-friendly disposal pathway (Chen et al., 2024).

b. Safe Disposal

The composite's stable structure and inert nature after regeneration ensure that it can be disposed of without releasing harmful substances, adhering to environmental safety standards (Ghaedi et al., 2025).

The composite's regeneration process is designed to align with sustainable practices:

I. Eco-Friendly Regeneration

Thermal and chemical regeneration methods generate minimal emissions and waste compared to producing new materials. Acidic or basic solutions used for chemical regeneration can often be recycled, further reducing waste.

II. Reduced Energy Consumption

The composite operates efficiently under sunlight, leveraging natural energy instead of industrial power sources, reducing the carbon footprint significantly.

3.3.3 Commercialization of ZnO-doped activated carbon-ammonia composite

a) Manufacturability

The ZnO-Doped Activated Carbon-Ammonia Composite relies on low-cost raw materials, such as activated carbon derived from bio-waste. These materials are known for their availability and affordability. Zinc oxide (ZnO) has been well-documented as an efficient catalyst for water treatment, supporting its industrial feasibility (Alprol et al., 2024a). The preparation process is simple and scalable, involving thermal drying at low temperatures compared to other industrial techniques. This feature allows for production using affordable industrial equipment.

b) Economic Feasibility and Cost

The composite compares favorably with traditional techniques like adsorption in terms of efficiency and cost. Studies have shown that the composite's reusability significantly reduces operational costs, as the material can be regenerated after multiple cycles (Lashaki et al., 2012). Additionally, the ability to use sunlight as the primary energy source during operation further reduces overall costs compared to the need for expensive artificial lighting.

c) Industrial Applications

The composite has demonstrated efficiency in treating industrial wastewater, particularly in industries that utilize dyes such as AR14, which is common in textiles, paper, and leather industries. The ZnO-based composite leverages its photocatalytic properties, which operate efficiently under sunlight, reducing reliance on additional energy sources (Alprol et al., 2024b). The composite effectively treats water contaminated with organic dyes that are difficult to break down using conventional methods.

d) Commercial Model

For commercialization, the composite can be produced in various forms, such as granules or films, to adapt to client needs across different industries. Studies have shown that the composite can be integrated into industrial wastewater treatment systems, such as photoreactors, to enhance water treatment efficiency and reduce operational costs (Mei et al., 2023; Sharma et al., 2024). Utilizing readily available and affordable materials like activated carbon and zinc oxide. Treating pollutants using sunlight instead of industrial energy sources. Compatibility with a wide range of industrial systems.

3.4 Adsorption isotherm

Isotherm models are fundamental tools in describing the equilibrium between a solute in solution and its adsorption on a solid surface (Abualnaja et al., 2021). They provide insights into the adsorption mechanisms and interactions at the molecular level. In this study, various isotherm models were applied to investigate the sorption equilibrium of Acid Red 14 onto AC-ZnO-NH³ composites (Table 2). By fitting the experimental data to these isotherm models, we can assess how well each model describes the adsorption process and predict the behavior of the system under different conditions.

TABLE 2 Adsorption isotherm model constants and correlation coefficients for acid red 14 onto AC-ZnO-NH³ composites.

Model	Variables	Values	R ²	
	1/n	1.686		
Henderson	K	0.014	0.99	
	q _e	1.30		
II-loss	1/n	0.143	0.022	
Halsey	K	6		
	q _e Exp	5.97		
Linearized Langmuir	$Ka \times 10^3$	1.92	0.50	
	q _e Pred	5.92		
Freundlich	1/n	6.988	0.022	
Freundiich	k _f	12.711	0.022	
II. dela I.	AHJ	0.05	0.22	
Harkins-Jura	ВНЈ	0.17		
	Q_m	5.16		
D-R isotherm	$K \times 10^6$	0.02 0.369		
	E	4.72		

The Henderson isotherm model showed the best fit to the experimental data, with an R^2 value of 0.99 (Figure 7d). The constants obtained were 1/n = 1.686, K = 0.014 and q_e predicted = 1.30 mg/g. This high correlation suggests that the Henderson model provides a highly accurate description of the adsorption of Acid Red 14 onto AC-ZnO-NH³. The 1/n value suggests a relatively high heterogeneity of the adsorption sites on the composite surface. The model implies that the adsorption process may involve multiple interactions between the dye molecules and the surface of the adsorbent. The high R^2 value (0.99) also indicates that this model captures both the linear and nonlinear behavior of the sorption process, making it a robust predictor for the adsorption capacity. The small K value (0.014) suggests a slow rate of adsorption equilibrium, indicating that the sorption process is somewhat gradual (Aragaw and Alene, 2022).

The Halsey isotherm had a significantly lower correlation coefficient ($R^2=0.022$), with constants: 1/n=0.143 and K=6. The poor fit of the Halsey model indicates that it is not suitable for describing the adsorption behavior of Acid Red 14 onto AC-ZnO-NH³ composites. The 1/n value of (0.143) suggests an extremely low heterogeneity, which may not reflect the real nature of the adsorption surface in this case. The large K value of (6) further suggests that the model predicts a fast adsorption process, which contradicts the actual experimental data.

The linearized Langmuir isotherm produced a moderate correlation, with an R^2 value of 0.50. The experimental and predicted values were q_e Exp = 5.97 mg/g, Ka $\times\,10^3$ = 1.92 and q_e Pred = 5.92 mg/g. The Langmuir isotherm assumes monolayer adsorption onto a surface with finite and identical sites, which might not entirely describe the system in this study. The moderate

 $\rm R^2$ value (0.50) shows that the model somewhat fits the experimental data but fails to capture all the complexities of the adsorption process, especially at higher concentrations. The closeness between the experimental and predicted values of $\rm q_e$ indicates that the Langmuir model reasonably predicts the maximum adsorption capacity, although it does not fully account for multi-layer adsorption or interaction between dye molecules (Acharya et al., 2024).

The Freundlich isotherm also performed poorly, with an R^2 value of 0.022. The constants obtained were 1/n = 6.988 and $k_f = 12.711$. This model, which is usually applied to heterogeneous surfaces, seems to overestimate the heterogeneity of the adsorption sites in this case (Rushton et al., 2005). The 1/n value of (6.988) suggests an unusual adsorption intensity, while the kf value of (12.711) indicates a high adsorption capacity, which is not supported by the experimental data. The low R^2 value further confirms that this model is not appropriate for the sorption of Acid Red 14 onto AC-ZnO-NH³.

The Harkins-Jura isotherm produced a relatively low correlation with an R² value of 0.22. The constants for AHJ = 0.05 and BHJ = 0.17. This model is used to describe multilayer adsorption and the presence of heterogeneous pore distribution (BASAR, 2006). The low correlation coefficient indicates that the Harkins-Jura model does not accurately describe the adsorption process for this system. The AHJ and BHJ values suggest that although the model accounts for multilayer adsorption, it does not fit well with the experimental data.

Based on the correlation coefficients (R² values) and the fit of the experimental data to each model, the Henderson isotherm was found to be the best-fitting model for describing the adsorption of Acid Red 14 onto AC-ZnO-NH³ composites. This model exhibited the highest R² value (0.99), indicating a highly accurate fit. The Langmuir isotherm, while reasonably fitting the maximum adsorption capacity, did not capture the complete behavior of the system, especially at higher dye concentrations. The Freundlich, Halsey, and Harkins-Jura models failed to adequately describe the adsorption process, as indicated by their low R² values.

Also, the rate of adsorption can be inferred from the constants obtained from the isotherm models. The K value in the Henderson model (0.014) suggests a relatively slow adsorption process, indicating that the system takes time to reach equilibrium. Conversely, the Halsey model predicted a much faster rate of adsorption (K = 6), but its low R² value suggests that this result is not reliable for this system. The Langmuir constant Ka \times 10³ = 1.92 also indicates moderate interaction strength between the adsorbent and the adsorbate, pointing to a reasonably quick but not immediate adsorption process (Khamseh et al., 2023).

The Dubinin–Radushkevich (D–R) isotherm provides insight into the nature of adsorption, specifically regarding the porosity of the adsorbent and the mean free energy of adsorption (Mohamed et al., 2020). It is often used to distinguish between physical and chemical adsorption based on the magnitude of the calculated adsorption energy (E), β parameter of the Dubinin Radushkovich isotherm was also obtained according to Equation 6, and the calculations presented in Table 2.

$$q_e = q_m \exp(-K\epsilon^2), \epsilon = RT \ln(1 + \frac{1}{C})$$
 (6)

where: q_m is the theoretical saturation capacity, K is a constant related to the adsorption energy, ϵ is the Polanyi potential, $E=\frac{1}{\sqrt{2K}}$ is the mean free energy (kJ/mol). The process can be classified into two groups according to the energy levels involved: chemical adsorption and physical adsorption (with high energy and low energy, respectively). The energy is between 8 and 168 kJ/mol in chemical adsorption and less than 8 kJ/mol in physical adsorption (Hu and Zhang, 2019). Understanding the nature of the adsorption process and how it affects the characteristics of the adsorbent surface is made easier by this classification.

However, the calculated adsorption energy (E = 4.72 kJ/mol) falls within the range of physical adsorption (< 8 kJ/mol), but approaches the threshold of chemical adsorption (Edet and Ifelebuegu, 2020). The relatively low q_m value ($q_m = 5.16 \, \text{mg g} - 1$). The low correlation coefficient ($R^2 = 0.369$) suggests a poor fit compared to other isotherm models such as Henderson. This intermediate energy implies that the AR14 adsorption onto AC-ZnO-NH³ may involve a hybrid mechanism, where initial physisorption is followed or assisted by localized chemisorption, particularly at functionalized or defectrich active sites.

In comparison with previous studies on dye adsorption, the dominance of the Henderson model here suggests that this specific system has a relatively high heterogeneity, which could be attributed to the unique properties of the AC-ZnO-NH³ composites. In other dye removal studies using materials like activated carbon, the Langmuir and Freundlich models often provided better fits, indicating monolayer or heterogeneous adsorption, respectively. However, the AC-ZnO-NH³ system appears to deviate from these trends due to its complex surface interactions.

3.5 Adsorption kinetics of acid red 14 dye onto AC-ZnO-NH³ composites

Understanding the adsorption kinetics is crucial for optimizing the efficiency and mechanism of dye removal using composite adsorbents like AC-ZnO-NH³. Kinetics provide insights into the rate at which the adsorption process occurs and the steps involved in the removal of the solute from the solution. This study examines the adsorption kinetics of Acid Red 14 dye using different kinetic models: pseudo first order, pseudo second order, and intraparticle diffusion models. These models help elucidate the reaction rate, adsorption mechanism, and diffusion behavior, enabling a deeper understanding of the system's performance.

The pseudo-first-order kinetic model, also known as the Lagergren model, is often used to describe the rate of adsorption of solutes onto solid surfaces, assuming that the rate of adsorption is directly proportional to the number of unoccupied adsorption sites (Revellame et al., 2020). In this study, the pseudo first-order model yielded in Table 3. The results showed that the q_e (0.19 mg/g) indicates the equilibrium adsorption capacity, which is relatively low in this model. The constant $K_1 \times 10^3 = 0.02$ reflects the rate of adsorption, suggesting a slow adsorption process for Acid Red 14.

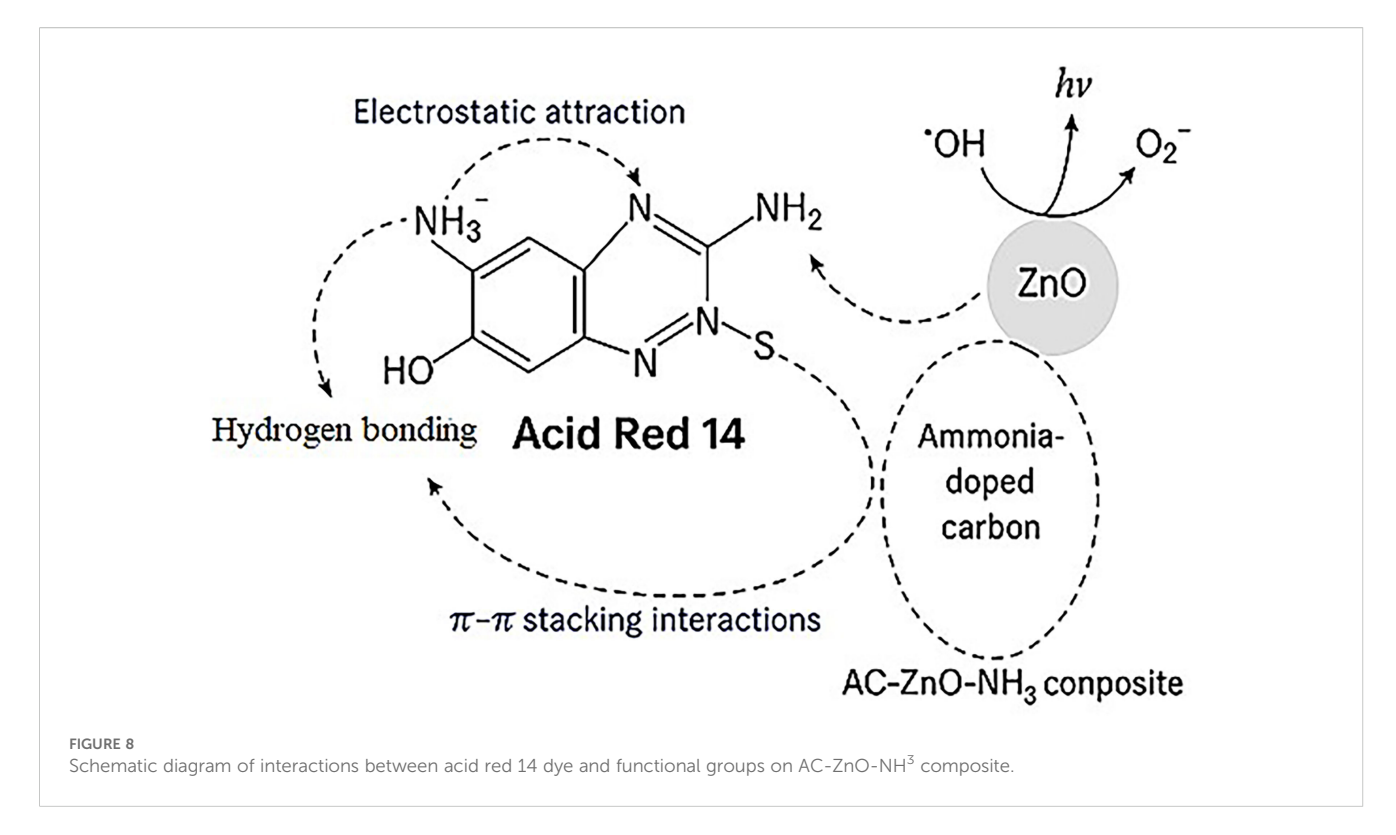
TABLE 3 Adsorption kinetics of acid red 14 dye onto AC-ZnO-NH³ composites.

Model	Variables	Values	R²	
Pseudo	q _e	0.19	0.788	
First Order	$K_1 \times 10^3$	0.02		
Pseudo	q _e	29.76	0.079	
Second Order	$k^2 \times 10^3$	33.60	0.978	
Intraparticle	K _{dif}	12.22	0.53	
Diffusion	С	1.87		
	β 0.70			
Elovich kinetic	LN (αβ)	17.44	0.147	
Elovich Kinetic	αβ	37451503.14		
	α	53791593.96		

This correlation coefficient ($R^2 = 0.788$) indicates a moderate fit of the experimental data to the pseudo first-order model, but it is not a perfect representation of the adsorption kinetics. In many dye adsorption studies, the pseudo first-order model tends to underestimate the experimental equilibrium capacity (q_e), particularly in cases where chemical adsorption is predominant (Al-Harby et al., 2021). The model is typically more suitable for systems where physical adsorption is the primary mechanism. However, in this study, the relatively low q_e and K_1 values suggest that the adsorption mechanism may not be purely physical, and other models may offer better insights into the adsorption process.

The pseudo second-order model assumes that the adsorption rate is controlled by the availability of adsorption sites and the square of the number of unoccupied sites. This model is often used to describe chemisorption, where the adsorption involves valence forces through the sharing or exchange of electrons between adsorbent and adsorbate (Bullen et al., 2021). In this study, the results of pseudo second-order model are presented in Table 3. The qe value (29.76 mg/g) from the pseudo second-order model is significantly higher than that of the pseudo first-order model, indicating that the system has a much higher equilibrium adsorption capacity when evaluated under this model. The higher k² value of (33.60) suggests a faster adsorption rate compared to the first-order model, indicating that the system reaches equilibrium more quickly. Moreover, the high correlation coefficient (R² = 0.978) demonstrates an excellent fit of the experimental data to the pseudo-second-order model. The pseudo second-order model is frequently observed to outperform the first-order model in adsorption studies, especially when the adsorption involves strong chemical bonds between the adsorbent and the adsorbate. The higher q_e and R² values in this study suggest that the adsorption of Acid Red 14 onto AC-ZnO-NH3 is primarily governed by chemisorption, involving strong interactions between the dye molecules and the composite surface.

The intraparticle diffusion model helps to assess whether diffusion within the pores of the adsorbent is the rate-limiting step in the adsorption process. This model is often used in



combination with other models to evaluate the diffusion mechanisms in porous materials (Hu et al., 2024). The $K_{\rm dif}$ value of (12.22 mg/g min^{0.5}) represents the diffusion rate constant, which reflects the rate at which the dye molecules diffuse into the pores of the AC-ZnO-NH³ composites. The C value (1.87) provides insight into the boundary layer effect, with higher values indicating a more significant influence of the boundary layer on the adsorption process. The relatively low R² value of (0.53) indicates that intraparticle diffusion does not solely control the overall rate of adsorption. The intraparticle diffusion model provides insights into the diffusion-controlled steps of the process, but the relatively low $K_{\rm dif}$ value (12.22 mg/g min^{0.5}) suggests that diffusion is not the rate-limiting step, and the adsorption process is controlled more by surface interactions and chemical bonding.

In many dye adsorption systems, intraparticle diffusion plays a significant role, but it is rarely the only mechanism controlling the rate of adsorption (Wang and Guo, 2022). The low R² value suggests that while intraparticle diffusion may be involved in the adsorption process of Acid Red 14 onto AC-ZnO-NH³, it is not the dominant rate-limiting step. Instead, other processes, such as surface adsorption or chemical interactions, likely play a more critical role.

When comparing the three kinetic models, it is evident that the pseudo second-order model provides the best fit for describing the adsorption kinetics of Acid Red 14 onto AC-ZnO-NH³ composites. This model not only has the highest R² value (0.978) but also predicts a much higher q_e value (29.76 mg/g), which aligns well with the experimental data. The high k^2 value suggests that the adsorption process is relatively fast and involves strong chemical interactions between the adsorbate and adsorbent. The pseudofirst-order model, on the other hand, provided a much lower q_e value (0.19 mg/g) and a weaker correlation ($R^2 = 0.788$), indicating

that it does not accurately capture the adsorption mechanism for this system. This model may be more suitable for systems where physical adsorption dominates, but it is not appropriate for the chemisorption-driven adsorption observed in this study (Al-Harby et al., 2021). The intraparticle diffusion model provides useful insights into the role of diffusion in the adsorption process, but its low correlation coefficient ($R^2 = 0.53$) suggests that it is not the dominant mechanism. While intraparticle diffusion likely contributes to the overall adsorption rate, it does not fully explain the observed behavior, and other mechanisms (such as surface adsorption or chemical bonding) must be considered (Rushton et al., 2005).

The Elovich model is frequently applied to describe the kinetics of chemisorption on heterogeneous surfaces, particularly in systems where the adsorption rate decreases exponentially with time due to an increase in surface coverage or activation barriers (Largitte and Pasquier, 2016). The model is expressed as Equation 7:

$$q_t = \frac{1}{\beta} \ln(\alpha \beta) + \frac{1}{\beta} \ln t \tag{7}$$

where: α (mg·g⁻¹·min⁻¹) is the initial adsorption rate and β (g·mg⁻¹) relates to the extent of surface coverage and activation energy for chemisorption.

In the present study, Table 3 presented the Elovich model which yielded that $\alpha = 5.38 \times 10^7 \, \mathrm{mg. g^{-1} \, min^{-1}}$, $\beta = 0.70 \, \mathrm{g.mg^{-1}}$. Despite the very high initial adsorption rate, the low correlation coefficient suggests that the Elovich model does not provide a strong fit to the experimental data ($R^2 = 0.147$). However, the value of β supports the presence of a chemisorption mechanism, potentially involving valency forces through sharing or exchange of electrons between the dye molecules and the composite surface (Sivashankar

et al., 2014). Most of the time, however, it was not possible to determine the relationship between the starting concentrations and the initial adsorption rate constant (α) by estimating its highest values at low initial concentrations. Furthermore, according to the computed β values, the activation energy of chemisorption and the number of sites available for adsorption rose as the initial metal ion concentrations increased, while non-linear fitting displayed the opposite trend, with decreasing β values (Shafiq et al., 2021).

3.6 Thermodynamic studies

Thermodynamic parameters provide important insights into the nature of adsorption processes, including whether the reaction is spontaneous, endothermic or exothermic, and the degree of randomness at the solid-liquid interface (Abualnaja et al., 2021). For the removal of Acid Red 14 dye using AC-ZnO-NH³ composites, thermodynamic analysis was conducted by determining key parameters such as Gibbs free energy (ΔG°), enthalpy (ΔH°), and entropy (ΔS°) over a range of temperatures as presented in Table 4S.

The Gibbs free energy change (ΔG°) provides information on the spontaneity of the adsorption process (Saha and Chowdhury, 2011). At temperatures (60–70 °C), ΔG° values are negative (-6.231 kJ/mol at 70 °C and -5.85 kJ/mol at 60 °C), suggesting that the adsorption process is spontaneous at elevated temperatures. This indicates that the adsorption of Acid Red 14 onto AC-ZnO-NH³ composites becomes more thermodynamically favorable as the temperature increases. The adsorption process is spontaneous as indicated by the negative ΔG° values.

The enthalpy change (ΔH°) is used to determine whether the process is endothermic (positive ΔH°) or exothermic (negative ΔH°). The positive enthalpy change ($\Delta H^{\circ} = 83.206$ kJ/mol) indicates that the adsorption of AR14 dye onto the AC-ZnO-NH³ composite is endothermic, meaning the process is favored by the absorption of heat (Li et al., 2024). The significant positive ΔH° value also supports the idea that chemical interactions (chemisorption) are the dominant adsorption mechanism, as these typically require more energy compared to physical adsorption (physisorption).

The entropy change (ΔS°) reflects the degree of disorder or randomness at the solid-liquid interface during the adsorption process (Saha and Chowdhury, 2011). In this study, the ΔS° value of -0.261 kJ/mol/K is negative, implying a decrease in system disorder, which can be attributed to the more ordered arrangement of dye molecules at the solid-liquid interface upon adsorption (Saha and Chowdhury, 2011).

This reduction in randomness suggests that the dye molecules form more organized and structured bonds with the adsorbent during the adsorption process, which aligns with the chemisorption mechanism implied by the positive ΔH° value. The negative entropy change could also indicate a restriction in the freedom of movement of dye molecules upon adsorption, which is typical for processes where specific interactions (such as chemical bonding) occur.

3.7 Mechanism for removing acid red 14 dye from aqueous solutions using ZnO-doped AC-NH₃ composites under sunlight

I) Building upon the characterization data (XRD, IR, SEM, EDX) for AC-ZnO-NH³, the XRD data reveals the presence of ZnO nanoparticles with a characteristic wurtzite structure within the composite, confirmed further by EDX analysis. SEM analysis confirms the porous structure of the activated carbon (AC) with integrated ZnO nanoparticles. The porous structure and high surface area provide numerous adsorption sites for dye molecules, leading to increased dye adsorption capacity. The IR analysis provides insights into functional groups as the broad peaks around 3000-3500 cm⁻¹ indicate the presence of hydroxyl (-OH) groups and amine (-NH) groups due to the ammonia doping. These groups create a more hydrophilic surface enhancing interaction with the aqueous dye solutions. The nitrogen functionalities also contribute to stronger interactions through hydrogen bonding. The presence of carbonyl (C=O) and amine (C-N) stretching vibrations within this region are crucial for the adsorption process, enhancing interactions between the composite surface and the dye molecules. The AR14 dye molecules, negatively charged due to sulfonate groups (-SO₃), are attracted to the composite surface through multiple mechanisms. Also, the NH3 doping enhances the surface basicity of the composite material, giving it a net positive charge. This attracts the negatively charged dye molecules, promoting initial adsorption. The hydroxyl (-OH) groups and amine (-NH) groups, identified by IR, create a favorable environment for hydrogen bonding with the dye's polar functional groups. The aromatic structures in both the activated carbon and the dye molecule allow for π - π interactions, enhancing adsorption (Figure 8).

II) Photocatalytic Activation

When exposed to sunlight, the ZnO absorbs photons, promoting electrons from the valence band to the conduction band, generating electron-hole pairs (e⁻/h⁺). The AC-NH₃ component helps to separate these charge carriers, reducing recombination and enhancing the photocatalytic efficiency. The photogenerated holes (h⁺) oxidize water (H²O) or hydroxide ions (OH⁻) to form hydroxyl radicals (•OH), which are highly reactive. The conduction band electrons (e⁻) can react with dissolved oxygen (O^2) to form superoxide radicals ($\bullet O^{2-}$). The reactive species ($\bullet OH$ and •O²⁻) attack the Acid Red 14 dye molecules, breaking down the dye's molecular structure into smaller, less harmful compounds. The degradation can involve a series of oxidation reactions, ultimately leading to the formation of simpler organic compounds and inorganic ions, such as CO2 and H2O. With sufficient exposure time and light intensity, the final products can be fully mineralized into carbon dioxide and water, effectively removing the dye from the solution.

III) From the isotherm, kinetics and thermodynamics study; the Henderson isotherm model provides a strong fit, suggesting high heterogeneity in the adsorption sites, reflecting the complex

interaction between the dye and composite. Besides, the pseudo second-order model offers the best fit, indicating the chemisorption process and rapid adsorption of AR14 onto the composite. The endothermic and spontaneous nature of the process, evident from the thermodynamic studies, indicates that chemical interactions play a significant role in adsorption.

IV) The Role of Ammonium and Functional Groups in the Composition of Zinc Oxide and Other Oxides for Dye Degradation

The efficiency of zinc oxide (ZnO) and other metal oxides in degrading dyes such as Acid Red 14 is significantly influenced by the incorporation of ammonium (NH³) and the presence of functional groups on their surfaces. These modifications enhance adsorption, photocatalysis, and the overall degradation process.

1. Role of Ammonium (NH³) in the Composition

Ammonium plays a pivotal role in modifying the properties of ZnO and other oxides, creating a more effective material for dye degradation (Rosado-Mendoza et al., 2020).

The key contributions are as follows:

a. Surface Basicity Enhancement

Ammonium doping introduces nitrogen atoms into the oxide lattice or surface, increasing the basicity of the material (Latham et al., 2021). Similarly, the basic surface interacts strongly with acidic dye molecules (Acid Red 14, which contains sulfonate groups -SO³⁻). This electrostatic attraction promotes better adsorption and facilitates subsequent degradation.

b. Generation of Active Sites

Ammonium doping introduces nitrogen-containing functional groups, such as amines (-NH or $-NH^2$), which act as additional adsorption sites for dye molecules (Travlou et al., 2016). These groups enhance the material's ability to capture and hold dyes, ensuring close interaction with photocatalytic or oxidative sites.

c. Improved Photocatalytic Activity

Nitrogen incorporation narrows the bandgap of ZnO and other oxides, making them more responsive to visible light. This increases the generation of reactive oxygen species (ROS) like hydroxyl radicals (\cdot OH) and superoxide anions (O_2^-), which degrade the dye more effectively under sunlight. Nitrogen doping also reduces electron-hole recombination, ensuring a higher photocatalytic efficiency.

2. Role of Functional Groups on the Surface

The functional groups present on the surface of ZnO or other oxides play a critical role in dye degradation by enhancing both adsorption and photocatalysis.

a. Hydroxyl Groups (-OH)

Hydroxyl groups on the surface of oxides act as key adsorption sites for dye molecules (Cui et al., 2022). They form hydrogen bonds with polar groups in the dye, facilitating strong adsorption.

During photocatalysis, surface hydroxyl groups generate hydroxyl radicals (\cdot OH) upon reacting with photo-generated holes (h⁺) (Xiang et al., 2011): OH⁻ + h⁺ \rightarrow ·OHThese hydroxyl radicals are highly reactive and attack the dye's chromophores, breaking them down into simpler, less toxic molecules like CO² and H²O.

b. Amine Groups (-NH or -NH²)

Amine groups, introduced via ammonium doping, enhance the interaction with dye molecules through electrostatic interactions and hydrogen bonding.

These groups also improve adsorption capacity, particularly for dyes with anionic structures like Acid Red 14.

c. Carbonyl (C=O) and Carboxyl Groups (-COOH)

Functional groups like carbonyl or carboxyl groups enhance the material's hydrophilicity and adsorption capacity. They interact with the dye molecules' polar functional groups, further stabilizing adsorption.

d. Zinc-Oxygen Bonds (Zn-O)

Zn-O bonds are essential for photocatalysis. They serve as the sites where electron-hole pairs are generated upon light irradiation. These bonds contribute to the production of ROS, which play a crucial role in breaking the azo bonds (-N=N-) in dyes (Phan et al., 2024).

3. Synergistic role of ammonium and functional groups

The combination of ammonium doping and functional groups significantly enhances the degradation process. Ammonium increases the number of active sites, while functional groups as: – OH and –NH² create specific interactions with dye molecules. Whereas, improved Photocatalytic Efficiency: Nitrogen doping improves the visible light activity of ZnO, while functional groups ensure the effective generation of ROS. Besides, reduction of Electron-Hole Recombination: Functional groups, especially nitrogen-based ones, stabilize charge carriers, ensuring more ROS are produced and utilized for dye degradation.

3.8 Assessment of water quality parameters before and after treatment

To evaluate the real-world applicability of the AC-ZnO-NH³ composite, several key water quality parameters were analyzed before and after treatment of dye-contaminated water (Table 5S) (Chander et al., 2024). The results demonstrate a significant improvement in water quality, indicating the material's high efficiency in degrading Acid Red 14 and reducing pollutant loads. The pH value increased from 4.2 to 6.9, indicating a shift from acidic to near-neutral conditions, which is favorable for environmental discharge (Chander et al., 2025). Color intensity (ADMI) was reduced by nearly 90%, from 1220 to 125, confirming the breakdown of chromophoric groups in the dye structure. Similarly, a noticeable reduction in total dissolved solids (TDS) was also observed, decreasing from 950 to 310 mg/L, suggesting the effective elimination of dissolved ions and dye-related residues (Butler and Ford, 2018). Turbidity, a measure of suspended particles and colloidal matter, improved significantly from 48 to 5.4 NTU, reflecting the removal of dye aggregates and particulate contaminants (Husen et al., 2024). Most importantly, the dye concentration decreased from 25 to 1.8 mg/L, achieving a removal efficiency of over 92%, highlighting the composite's dual functionality in adsorption and sunlight-driven photodegradation

(Chander and Gupta, 2025). These results collectively demonstrate the potential of the AC-ZnO-NH³ composite for application in treating textile or industrial wastewater under environmentally friendly and cost-effective conditions using natural sunlight as the driving force.

3.9 Environmental aspects of the AC-ZnO-NH³ composite

The development and application of multifunctional materials for wastewater treatment must account not only for performance efficiency but also for environmental safety (Nain et al., 2025). In the case of the AC-ZnO-NH³ composite, several important factors mitigate its potential environmental impact and support its feasibility for large-scale use.

I. Carbon-Based Support: Inert and Non-Toxic Framework

Activated carbon (AC), which forms the structural backbone of the composite, is well established as a safe and environmentally benign material. Its widespread use in air and water purification is attributed to its high porosity, chemical inertness, and non-toxic nature (Hasanzadeh et al., 2020). By embedding ZnO and NH³ functionalities within the porous AC matrix, the composite benefits from a stable and inert support that resists leaching and contributes minimal ecological burden.

II. ZnO Stability and Reuse Potential

While zinc oxide (ZnO) exhibits desirable photocatalytic properties, it is known to exhibit partial solubility under certain conditions, particularly in acidic media or upon prolonged irradiation. This dissolution may release Zn²⁺ ions, which, in excess, could impact aquatic systems. This structural confinement limits its direct exposure to the aqueous phase and significantly reduces the potential for uncontrolled leaching. Moreover, the material is designed for multiple regeneration cycles, as shown in the study's reusability tests. Encouraging the repeated use of the composite instead of singleuse applications minimizes environmental release and supports a circular material lifecycle.

III. Controlled Use of Ammonia: Avoiding Free Ammonia Pollution

Ammonia doping enhances the surface basicity and nitrogen functionalization of the carbon matrix, improving the composite's adsorption capacity for acidic dyes like AR14. However, if not properly controlled, excess free ammonia in the system may contribute to secondary pollution and eutrophication risks in aquatic environments. In this study, ammonia is used in a controlled volume (3.5 mL of 15% v/v solution), followed by thorough washing and heat treatment to remove any residual free ammonia. Therefore, the final composite is largely free from unbound ammonia, minimizing this concern. Nonetheless, monitoring of free ammonia in effluents post-treatment should be considered in field applications.

IV. Structural Confinement of ZnO within Carbon Matrix

To further enhance environmental compatibility, the design strategy of this composite intentionally utilizes the mesoporous structure of activated carbon to physically and chemically anchor ZnO nanoparticles (Sreenan et al., 2025). The high internal surface area and functional groups on AC allow for strong interactions with ZnO particles, reducing their mobility. This immobilization within pores or via chemical bonding not only improves photocatalytic stability under solar irradiation but also reduces the risk of ZnO detachment or dispersion into treated water.

4 Conclusion

This study demonstrated the successful development and application of a ZnO-doped activated carbon-ammonia (AC-ZnO-NH³) composite for the efficient sunlight-driven degradation of Acid Red 14 dve. The composite exhibited synergistic photocatalytic and adsorptive behavior, benefiting from the high surface area of activated carbon, the photoactivity of ZnO, and enhanced surface basicity introduced by ammonia doping. Key findings revealed that the optimal dye removal (95.5%) was achieved at pH 3 with 0.18 g of catalyst under sunlight, confirming the high efficiency of the system. The presence of H²O² significantly enhanced photocatalytic performance, reducing the dye's half-life and accelerating degradation through ROS formation. Kinetic data fitted well with the pseudo-second-order model, and the Henderson isotherm best described the equilibrium data, suggesting a chemisorption mechanism on heterogeneous sites. The process was spontaneous and endothermic, indicating enhanced removal at elevated temperatures. The composite retained reasonable activity across three regeneration cycles, confirming partial reusability. The novelty of this work lies in the integration of low-cost materials into a multifunctional composite capable of simultaneously adsorbing and degrading persistent dyes under eco-friendly solar irradiation. These findings highlight the potential of AC-ZnO-NH³ as a scalable, sustainable, and cost-effective solution for real-world wastewater treatment applications.

Data availability statement

The original contributions presented in the study are included in the article/Supplementary Material. Further inquiries can be directed to the corresponding authors.

Author contributions

AE: Methodology, Visualization, Formal Analysis, Conceptualization, Validation, Supervision, Writing – original draft, Data curation, Investigation, Writing – review & editing, Resources. AB: Writing – review & editing, Investigation, Methodology. SA: Writing – review & editing, Formal Analysis, Data curation, Funding acquisition, Investigation, Conceptualization. EE-H: Visualization, Project administration, Software, Funding acquisition, Writing – review & editing. MA: Conceptualization, Visualization, Funding

acquisition, Software, Writing – review & editing, Investigation, Formal Analysis, Validation, Data curation.

Funding

The author(s) declare financial support was received for the research and/or publication of this article. The authors express their gratitude to the support of Princess Nourah bint Abdulrahman University Researchers Supporting Project number (PNURSP2025R58), Princess Nou-rah bint Abdulrahman University, Riyadh, Saudi Arabia.

Conflict of interest

The authors declare that the research was conducted in the absence of any commercial or financial relationships that could be construed as a potential conflict of interest.

Generative AI statement

The author(s) declare that no Generative AI was used in the creation of this manuscript.

Any alternative text (alt text) provided alongside figures in this article has been generated by Frontiers with the support of artificial intelligence and reasonable efforts have been made to ensure accuracy, including review by the authors wherever possible. If you identify any issues, please contact us.

Publisher's note

All claims expressed in this article are solely those of the authors and do not necessarily represent those of their affiliated organizations, or those of the publisher, the editors and the reviewers. Any product that may be evaluated in this article, or claim that may be made by its manufacturer, is not guaranteed or endorsed by the publisher.

Supplementary material

The Supplementary Material for this article can be found online at: https://www.frontiersin.org/articles/10.3389/fmars.2025.1624235/full#supplementary-material

References

Abdallah, M. A. M., and Alprol, A. E. (2024). Utilization of aquatic biomass as biosorbent for sustainable production of high surface area, nano-microporous, for removing two dyes from wastewater. *Sci. Rep.* 14, 4471. doi: 10.1038/s41598-024-54539-2

Abd El-Hamid, H. T., AlProl, A. E., and Hafiz, M. A. (2022). The efficiency of adsorption modelling and Plackett-Burman design for remediation of crystal violet by Sargassum latifolium. *Biocatal Agric. Biotechnol.* 44, 102459. doi: 10.1016/j.bcab.2022.102459

Abo El-Magd, A. E.-A., Gedamy, Y., and El.shahed, A. (2022). Removal of zinc ions from aqueous solutions and groundwater using activated carbon as ion exchange resin. *Egypt J. Chem.* doi: 10.21608/ejchem.2022.65510.4298

Abualnaja, K. M., Alprol, A. E., Ashour, M., and Mansour, A. T. (2021). Influencing multi-walled carbon nanotubes for the removal of ismate violet 2R dye from wastewater: isotherm, kinetics, and thermodynamic studies. *Appl. Sci.* 11, 4786. doi: 10.3390/app11114786

Acharya, A., Jeppu, G., Girish, C. R., Prabhu, B., Murty, V. R., Martis, A. S., et al. (2024). Adsorption of arsenic and fluoride: Modeling of single and competitive adsorption systems. *Heliyon* 10, e31967. doi: 10.1016/j.heliyon.2024.e31967

Aleboyeh, A., Daneshvar, N., and Kasiri, M. B. (2008). Optimization of C.I. Acid Red 14 azo dye removal by electrocoagulation batch process with response surface methodology. *Chem. Eng. Process.: Process. Intensification* 47, 827–832. doi: 10.1016/j.cep.2007.01.033

Al-Harby, N. F., Albahly, E. F., and Mohamed, N. A. (2021). Kinetics, isotherm and thermodynamic studies for efficient adsorption of congo red dye from aqueous solution onto novel cyanoguanidine-modified chitosan adsorbent. *Polymers (Basel)* 13, 4446. doi: 10.3390/polym13244446

Al Prol, A. E. (2019). Study of environmental concerns of dyes and recent textile effluents treatment technology: A review. *Asian J. Fish. Aquat. Res.* 3 (2), 1–18. doi: 10.9734/ajfar/2019/v3i230032

Alprol, A. E., Abu-Saied, M., Thabet, W. M., Abdelwahab, O., and El-Ghaffar, M. A. A. (2024c). Melamine-maleic acid polyamide adduct/polyacrylonitrile nanofibers as a novel adsorbent for removal of methyelene blue dye from aqueous solutions. *Water Air Soil pollut*. 235, 425. doi: 10.1007/s11270-024-07180-8

Alprol, A. E., Eleryan, A., Abouelwafa, A., Gad, A. M., and Hamad, T. M. (2024a). Green synthesis of zinc oxide nanoparticles using Padina pavonica extract for efficient photocatalytic removal of methylene blue. *Sci. Rep.* 14, 32160. doi: 10.1038/s41598-024-80757-9

Alprol, A. E., ElSheikh, M. A., Abdel-Salam, E. M., and Khairy, H. M. (2024b). Synergistic removal of acid red 73 dye from wastewater using a novel chitosan-blue-

green algae composite: adsorption and photocatalytic degradation. Rend. Lincei Sci. Fis. Nat. doi: 10.1007/s12210-024-01264-7

Alprol, A. E., Mansour, A. T., Abdelwahab, A. M., and Ashour, M. (2023a). Advances in green synthesis of metal oxide nanoparticles by marine algae for wastewater treatment by adsorption and photocatalysis techniques. *Catalysts* 13, 888. doi: 10.3390/catal13050888

Alprol, A. E., Mansour, A. T., El-Beltagi, H. S., and Ashour, M. (2023b). Algal extracts for green synthesis of zinc oxide nanoparticles: promising approach for algae bioremediation. *Materials* 16, 2819. doi: 10.3390/ma16072819

Alzahrani, E. A., Nabi, A., Kamli, M. R., Albukhari, S. M., Althabaiti, S. A., Al-Harbi, S. A., et al. (2023). Facile green synthesis of znO NPs and plasmonic ag-supported znO nanocomposite for photocatalytic degradation of methylene blue. *Water (Basel)* 15, 384. doi: 10.3390/w15030384

Aragaw, T. A., and Alene, A. N. (2022). A comparative study of acidic, basic, and reactive dyes adsorption from aqueous solution onto kaolin adsorbent: Effect of operating parameters, isotherms, kinetics, and thermodynamics. *Emerg. Contam.* 8, 59–74. doi: 10.1016/j.emcon.2022.01.002

Bano, K., Mittal, S. K., Singh, P. P., and Kaushal, S. (2021). Sunlight driven photocatalytic degradation of organic pollutants using a MnV $_2$ O $_6/\rm{BiVO}$ $_4$ heterojunction: mechanistic perception and degradation pathways. Nanoscale. Adv. 3, 6446–6458. doi: 10.1039/D1NA00499A

Barjasteh-Askari, F., Davoudi, M., Dolatabadi, M., and Ahmadzadeh, S. (2021). Iron-modified activated carbon derived from agro-waste for enhanced dye removal from aqueous solutions. *Helivon* 7, e07191. doi: 10.1016/j.helivon.2021.e07191

BASAR, C. (2006). Applicability of the various adsorption models of three dyes adsorption onto activated carbon prepared waste apricot. *J. Hazard. Mater.* 135, 232–241. doi: 10.1016/j.jhazmat.2005.11.055

Bullen, J. C., Saleesongsom, S., Gallagher, K., and Weiss, D. J. (2021). A revised pseudo-second-order kinetic model for adsorption, sensitive to changes in adsorbate and adsorbent concentrations. *Langmuir* 37, 3189–3201. doi: 10.1021/acs.langmuir.1c00142

Butler, B. A., and Ford, R. G. (2018). Evaluating relationships between total dissolved solids (TDS) and total suspended solids (TSS) in a mining-influenced watershed. *Mine Water Environ.* 37, 18–30. doi: 10.1007/s10230-017-0484-y

Chadi, N. E., Merouani, S., Hamdaoui, O., Bouhelassa, M., and Ashokkumar, M. (2019). H $_2$ O $_2$ /periodate (IO $_4$ $^-$): a novel advanced oxidation technology for the degradation of refractory organic pollutants. *Environ. Sci. (Camb)* 5, 1113–1123. doi: 10.1039/C9EW00147F

- Chander, S., and Gupta, A. (2025). Fabrication of mango-leaf biowaste mediated green magnetite (Fe3O4@MBE NPs) and modified EDTA/Fe3O4@MBE NCs for enhanced heavy metals sequestration: Characterisation, simulation modelling, mechanism, cost-effectiveness and electroplating wastewater performance. Sep. Purif. Technol. 358, 130246. doi: 10.1016/j.seppur.2024.130246
- Chander, S., Lodha, A., Veer, K., and Gupta, A. (2024). Enhanced methylene blue dye sequestration by carbon-embedded mesoporous zinc oxide nanoparticles fabricated utilizing Aloe barbadensis miller biowaste: Batch optimization, simulation modeling, and textile effluent feasibility. *Mater. Today Commun.* 40, 110107. doi: 10.1016/j.mtcomm.2024.110107
- Chander, S., Yadav, S., Singh, R., Rai Sharma, H., and Gupta, A. (2025). Sequestration of Ni2+ and Zn2+ utilising agricultural biowaste-based amorphous M–SiO2 and modified green M–SiO2/Fe3O4 nano-adsorbents: Modelling and electroplating wastewater performance. *J. Ind. Eng. Chem.* 145, 303–325. doi: 10.1016/j.jiec.2024.10.027
- Chen, L., Yang, M., Chen, Z., Xie, Z., Huang, L., Osman, A. I., et al. (2024). Conversion of waste into sustainable construction materials: A review of recent developments and prospects. *Mater. Today Sustainability* 27, 100930. doi: 10.1016/j.mtsust.2024.100930
- Cheng, S., Wang, T., Chu, L., Li, J., and Zhang, L. (2024). Preparation of nitrogen-doped activated carbon used for catalytic oxidation removal of H2S. *Sci. Total Environ.* 915, 170073. doi: 10.1016/j.scitotenv.2024.170073
- Cui, T., Su, Y., Fu, X., Zhu, Y., and Zhang, Y. (2022). The key role of surface hydroxyls on the activity and selectivity in photocatalytic degradation of organic pollutants and NO removal. *J. Alloys Compd.* 921, 165931. doi: 10.1016/j.jallcom.2022.165931
- Daneshvar, N., Salari, D., and Khataee, A. R. (2003). Photocatalytic degradation of azo dye acid red 14 in water: investigation of the effect of operational parameters. *J. Photochem. Photobiol. A Chem.* 157, 111–116. doi: 10.1016/S1010-6030(03)00015-7
- Dihom, H. R., Al-Shaibani, M. M., Radin Mohamed, R. M. S., Al-Gheethi, A. A., Sharma, A., and Bin Khamidun, M. H. (2022). Photocatalytic degradation of disperse azo dyes in textile wastewater using green zinc oxide nanoparticles synthesized in plant extract: A critical review. *J. Water Process. Eng.* 47, 102705. doi: 10.1016/j.jwpe.2022.102705
- Dong, C., Fang, W., Yi, Q., and Zhang, J. (2022). A comprehensive review on reactive oxygen species (ROS) in advanced oxidation processes (AOPs). *Chemosphere* 308, 136205. doi: 10.1016/j.chemosphere.2022.136205
- Edet, U. A., and Ifelebuegu, A. O. (2020). Kinetics, isotherms, and thermodynamic modeling of the adsorption of phosphates from model wastewater using recycled brick waste. *Processes* 8, 665. doi: 10.3390/pr8060665
- El-Fenjary, A. E., Abdel-Lateef, M., Mohran, H., and Elrouby, M. (2024). Synergetic effect of activated carbon and zero-valent iron for removal of nitrate-polluted potable water. *Sohag. J. Sci.* 9, 531–537. doi: 10.21608/sjsci.2024.288727.1202
- Frierdich, A. J., and Catalano, J. G. (2012). Distribution and speciation of trace elements in iron and manganese oxide cave deposits. *Geochim. Cosmochim. Acta* 91, 240–253. doi: 10.1016/j.gca.2012.05.032
- Fu, Y., and Manthiram, A. (2012). Core-shell structured sulfur-polypyrrole composite cathodes for lithium-sulfur batteries. *RSC Adv.* 2, 5927. doi: 10.1039/c2ra20393f
- Ghaedi, S., Rajabi, H., Hadi Mosleh, M., and Sedighi, M. (2025). MOF biochar composites for environmental protection and pollution control. *Bioresour. Technol.* 418, 131982. doi: 10.1016/j.biortech.2024.131982
- Ghoneim, M. M., El-Desoky, H. S., El-Moselhy, K. M., Amer, A., Abou El-Naga, E. H., Mohamedein, L. I., et al. (2014). Removal of cadmium from aqueous solution using marine green algae, Ulva lactuca. *Egypt J. Aquat. Res.* 40, 235–242. doi: 10.1016/j.ejar.2014.08.005
- Groeneveld, I., Kanelli, M., Ariese, F., and van Bommel, M. R. (2023). Parameters that affect the photodegradation of dyes and pigments in solution and on substrate An overview. *Dyes Pigments* 210, 110999. doi: 10.1016/j.dyepig.2022.110999
- Hasanzadeh, M., Simchi, A., and Shahriyari Far, H. (2020). Nanoporous composites of activated carbon-metal organic frameworks for organic dye adsorption: Synthesis, adsorption mechanism and kinetics studies. *J. Ind. Eng. Chem.* 81, 405–414. doi: 10.1016/j.jiec.2019.09.031
- Hekimoğlu, G., Sarı, A., Gencel, O., Tyagi, V. V., and Sharma, R. K. (2023). Activated carbon/expanded graphite hybrid structure for development of nonadecane based composite PCM with excellent shape stability, enhanced thermal conductivity and heat charging-discharging performance. *Thermal Sci. Eng. Prog.* 44, 102081. doi: 10.1016/j.tsep.2023.102081
- Hu, Q., Ma, S., He, Z., Liu, H., and Pei, X. (2024). A revisit on intraparticle diffusion models with analytical solutions: Underlying assumption, application scope and solving method. *J. Water Process. Eng.* 60, 105241. doi: 10.1016/j.jwpe.2024.105241
- Hu, Q., and Zhang, Z. (2019). Application of Dubinin–Radushkevich isotherm model at the solid/solution interface: A theoretical analysis. *J. Mol. Liq.* 277, 646–648. doi: 10.1016/j.molliq.2019.01.005
- Husen, A. K., Bidira, F., Bekel, E. A., Tegegn, M., Desta, W. M., and Asaithambi, P. (2024). Color, COD, and turbidity removal from surface water by using linseed and alum coagulants: optimization through response surface methodology. *Appl. Water Sci.* 14, 203. doi: 10.1007/s13201-024-02240-0

- Husien, S., El-taweel, R. M., Salim, A. I., Fahim, I. S., Said, L. A., and Radwan, A. G. (2022). Review of activated carbon adsorbent material for textile dyes removal: Preparation, and modelling. *Curr. Res. Green Sustain. Chem.* 5, 100325. doi: 10.1016/icrgsc.2022.100325
- Iyyappan, J., Gaddala, B., Gnanasekaran, R., Gopinath, M., Yuvaraj, D., and Kumar, V. (2024). Critical review on wastewater treatment using photo catalytic advanced oxidation process: Role of photocatalytic materials, reactor design and kinetics. *Case Stud. Chem. Environ. Eng.* 9, 100599. doi: 10.1016/j.cscee.2023.100599
- Khamseh, A. A. G., Ghorbanian, S. A., Amini, Y., and Shadman, M. M. (2023). Investigation of kinetic, isotherm and adsorption efficacy of thorium by orange peel immobilized on calcium alginate. *Sci. Rep.* 13, 8393. doi: 10.1038/s41598-023-35629-7
- Khan, S., Noor, T., Iqbal, N., and Yaqoob, L. (2024). Photocatalytic dye degradation from textile wastewater: A review. ACS Omega 9, 21751–21767. doi: 10.1021/ acsomega.4c00887
- Kumar Biswal, A., Sahoo, M., Kumar Suna, P., Panda, L., Lenka, C., and Kumari Misra, P. (2022). Exploring the adsorption efficiency of a novel cellulosic material for removal of food dye from water. *J. Mol. Liq.* 350, 118577. doi: 10.1016/j.molliq.2022.118577
- Kume, A. (2017). Importance of the green color, absorption gradient, and spectral absorption of chloroplasts for the radiative energy balance of leaves. *J. Plant Res.* 130, 501–514. doi: 10.1007/s10265-017-0910-z
- Lal, M., Chander, S., Sharma, P., and Ram, C. (2025). Synthesis and characterization of Nd-TiO $_2$ and Nd-ZnO nanostructures for photocatalytic degradation of textile wastewater. *Vietnam J. Chem.* 63, 324–337. doi: 10.1002/vjch.202400089
- Largitte, L., and Pasquier, R. (2016). A review of the kinetics adsorption models and their application to the adsorption of lead by an activated carbon. *Chem. Eng. Res. Des.* 109, 495–504. doi: 10.1016/j.cherd.2016.02.006
- Lashaki, M. J., Fayaz, M., Wang, H. H., Hashisho, Z., Philips, J. H., Anderson, J. E., et al. (2012). Effect of adsorption and regeneration temperature on irreversible adsorption of organic vapors on beaded activated carbon. *Environ. Sci. Technol.* 46, 4083–4090. doi: 10.1021/es3000195
- Latham, K. G., Forghani, M., Dose, W. M., Allen, J. A., and Donne, S. W. (2021). Influence of counter ions of ammonium for nitrogen doping and carbon properties in hydrothermal carbonization: characterization and supercapacitor performance. *Mater. Adv.* 2, 384–397. doi: 10.1039/D0MA00601G
- Lee, S.-M., Lee, S.-H., and Roh, J.-S. (2021). Analysis of activation process of carbon black based on structural parameters obtained by XRD analysis. *Crystals (Basel)* 11, 153. doi: 10.3390/cryst11020153
- León, A., Reuquen, P., Garín, C., Segura, R., Vargas, P., Zapata, P., et al. (2017). FTIR and raman characterization of tiO2 nanoparticles coated with polyethylene glycol as carrier for 2-methoxyestradiol. *Appl. Sci.* 7, 49. doi: 10.3390/app7010049
- Li, H., Li, T., Zhang, T., Zhu, J., Deng, W., and He, D. (2022a). Construction and adsorption performance study of GO-CNT/activated carbon composites for high efficient adsorption of pollutants in wastewater. *Polymers (Basel)* 14, 4951. doi: 10.3390/polym14224951
- Li, S., Tan, X., Li, H., Gao, Y., Wang, Q., Li, G., et al. (2022b). Investigation on pore structure regulation of activated carbon derived from sargassum and its application in supercapacitor. *Sci. Rep.* 12, 10106. doi: 10.1038/s41598-022-14214-w
- Li, X., Zhou, W., Chen, H., Zhang, Z., Jiang, M., Liu, P., et al. (2024). Multi-hierarchical assemble nano-fibrous dressing for burn wound ultra-fast healing with dynamical exudate regulation, thermal management, and non-leaching sterilisation. doi: 10.2139/ssrn.4836492
- Liang, Y., Yuan, F., Xu, X., Wang, X., Hu, H., and Ou, J. Z. (2023). Bioinspired polydopamine-sheathed carbon nanotubes as environmentally safe, efficient, and durable adsorbents for organic pollutant capturing via hydrogen bonding. *Carbon N Y* 214, 118354. doi: 10.1016/j.carbon.2023.118354
- Ma, X., Albertsma, J., Gabriels, D., Horst, R., Polat, S., Snoeks, C., et al. (2023). Carbon monoxide separation: past, present and future. *Chem. Soc. Rev.* 52, 3741–3777. doi: 10.1039/D3CS00147D
- Mansour, A. T., Alprol, A. E., Khedawy, M., Abualnaja, K. M., Shalaby, T. A., Rayan, G., et al. (2022). Green synthesis of zinc oxide nanoparticles using red seaweed for the elimination of organic toxic dye from an aqueous solution. *Materials* 15, 5169. doi: 10.3390/ma15155169
- Mao, Y., Cai, B., Huang, M., Liu, X., Zhang, W., and Ma, Z. (2023). A sustainable preparation strategy for the nitrogen-doped hierarchical biochar with high surface area for the enhanced removal of organic dye. *Biochar* 5, 70. doi: 10.1007/s42773-023-00269-z
- Marotti, R. (2004). Bandgap energy tuning of electrochemically grown ZnO thin films by thickness and electrodeposition potential. *Solar Energy Mater. Solar Cells* 82, 85–103. doi: 10.1016/j.solmat.2004.01.008
- Mei, J., Gao, X., Zou, J., and Pang, F. (2023). Research on photocatalytic wastewater treatment reactors: design, optimization, and evaluation criteria. *Catalysts* 13, 974. doi: 10.3390/catal13060974
- Mohamed, G., Rashwan, W., El-Nabarawy, T., and El-Hendawy, A. N. (2020). Removal of basic dyes from aqueous solution onto H2SO4-modified rice husk. *Egypt J. Chem.* doi: 10.21608/ejchem.2020.39613.2807

Nain, K., Chander, S., Bansal, S., and Bhukal, S. (2025). Fabrication of BMIM-PF6 modified mesoporous ZnO-IL and CuO-IL NMs for CV dye adsorption: Modeling, mechanism, and textile effluent decolourisation feasibility. *J. Mol. Struct.* 1335, 141963. doi: 10.1016/j.molstruc.2025.141963

Nessaibia, M., Ghodbane, H., Djaghout, I., Fetimi, A., Merouani, S., Alam, M., et al. (2023). Evaluation of the potentiality of the H $_2$ O $_2$ /IO $_4$ $^-$ process for the removal of acid orange 10 from the liquid phase: experimental investigation coupled with numerical analysis using the box–behnken design. *Ind. Eng. Chem. Res.* 62, 14167–14176. doi: 10.1021/acs.iecr.3c01938

Oliveira, E., Bértolo, E., Núñez, C., Pilla, V., Santos, H. M., Fernández-Lodeiro, J., et al. (2018). Green and red fluorescent dyes for translational applications in imaging and sensing analytes: A dual-color flag. *ChemistryOpen* 7, 9–52. doi: 10.1002/open.201700135

Pasti-Grigsby, M. B., Paszczynski, A., Goszczynski, S., Crawford, D. L., and Crawford, R. L. (1992). Influence of aromatic substitution patterns on azo dye degradability by Streptomyces spp. and Phanerochaete chrysosporium. *Appl. Environ. Microbiol.* 58, 3605–3613. doi: 10.1128/aem.58.11.3605-3613.1992

Phan, K.-H., Le, L.-T., Ninh, T.-T. N., Tran, C.-S., Nguyen, T.-T., Nguyen, D.-T.-D., et al. (2024). Decolorization and degradation of azo dyes in thermophilic biological wastewater treatment process: A mini-review. *Case Stud. Chem. Environ. Eng.* 10, 101018. doi: 10.1016/j.cscee.2024.101018

Pulido Melián, E., González Díaz, O., Doña Rodríguez, J. M., Colón, G., Araña, J., Herrera Melián, J., et al. (2009). ZnO activation by using activated carbon as a support: Characterisation and photoreactivity. *Appl. Catal A Gen.* 364, 174–181. doi: 10.1016/j.apcata.2009.05.042

Qu, T., Yao, X., Owens, G., Gao, L., and Zhang, H. (2022). A sustainable natural clam shell derived photocatalyst for the effective adsorption and photodegradation of organic dyes. *Sci. Rep.* 12, 2988. doi: 10.1038/s41598-022-06981-3

Raha, S., and Ahmaruzzaman, Md. (2022). ZnO nanostructured materials and their potential applications: progress, challenges and perspectives. *Nanoscale. Adv.* 4, 1868–1925. doi: 10.1039/D1NA00880C

Rahmani, Z., Kermani, M., Gholami, M., Jafari, A. J., and Mahmoodi, N. M. (2012). Effectiveness of photochemical and sonochemical processes in degradation of Basic Violet 16 (BV16) dye from aqueous solutions. *Iranian J. Environ. Health Sci. Eng.* 9, 14. doi: 10.1186/1735-2746-9-14

Rashidi, S., Soleiman-Beigi, M., and Kohzadi, H. (2024). Rapid and efficient removal of water-soluble dyes via natural asphalt oxide as a new carbonaceous super adsorbent; NA-oxide synthesis and characterization. *Sci. Rep.* 14, 24384. doi: 10.1038/s41598-024-75106-9

Revellame, E. D., Fortela, D. L., Sharp, W., Hernandez, R., and Zappi, M. E. (2020). Adsorption kinetic modeling using pseudo-first order and pseudo-second order rate laws: A review. *Clean Eng. Technol.* 1, 100032. doi: 10.1016/j.clet.2020.100032

Rosado-Mendoza, M., Casanova, D., and Oliva, A. I. (2020). Role of ammonia on the growth mechanism of znO films deposited at ambient temperature. ECS J. Solid State Sci. Technol. 9, 103002. doi: 10.1149/2162-8777/abc05b

Rushton, G. T., Karns, C. L., and Shimizu, K. D. (2005). A critical examination of the use of the Freundlich isotherm in characterizing molecularly imprinted polymers (MIPs). *Anal. Chim. Acta* 528, 107–113. doi: 10.1016/j.aca.2004.07.048

Saha, P., and Chowdhury, S. (2011). "Insight into adsorption thermodynamics," in $\it Thermodynamics$ (InTech). doi: 10.5772/13474

Saito, K., Xu, T., and Ishikita, H. (2022). Correlation between C=O stretching vibrational frequency and p K a shift of carboxylic acids. J. Phys. Chem. B 126, 4999–5006. doi: 10.1021/acs.jpcb.2c02193

Shafiq, M., Alazba, A. A., and Amin, M. T. (2021). Kinetic and isotherm studies of ni2+ and pb2+ Adsorption from synthetic wastewater using eucalyptus camdulensis—Derived biochar. Sustainability 13, 3785. doi: 10.3390/su13073785

Sharma, A., Yano, M., Zhang, C., Ming, J., Sun, X., Zhu, Y., et al. (2024). Efficient and stable immobilization of TiO2-based composite photocatalytic system for separation and purification of organic pollutants in wastewater under solar light. *J. Photochem. Photobiol. A Chem.* 452, 115549. doi: 10.1016/j.jphotochem.2024.115549

Singh, B. J., Chakraborty, A., and Sehgal, R. (2023a). A systematic review of industrial wastewater management: Evaluating challenges and enablers. *J. Environ. Manag.* 348, 119230. doi: 10.1016/j.jenvman.2023.119230

Singh, K., Lohchab, R. K., Kumar, V., and Kumar, A. (2023b). Degradation of ammonaical nitrogen (NH3-N) in leachate by zinc oxide loaded activated carbon: Process parameters modelling and optimization through RSM design. *Bioresour. Technol. Rep.* 24, 101602. doi: 10.1016/j.biteb.2023.101602

Sivashankar, R., Sathya, A. B., Vasantharaj, K., and Sivasubramanian, V. (2014). Magnetic composite an environmental super adsorbent for dye sequestration – A review. *Environ. Nanotechnol. Monit. Manag.* 1–2, 36–49. doi: 10.1016/j.emmm.2014.06.001

Sreenan, B., Kafil, V., Hunt, T., Shin, S. H. R., Brennan, A. A., Thallapally, P. K., et al. (2025). Luminescent znO-carbon hybrid nanomaterials: synthesis, characterization, emission mechanism, and applications. *ACS Appl. Optical. Mater.* 3, 698–711. doi: 10.1021/acsaom.4c00509

Suresh, D., Nethravathi, P. C., Udayabhanu, Rajanaika, H., Nagabhushana, H., and Sharma, S. C. (2015). Green synthesis of multifunctional zinc oxide (ZnO) nanoparticles using Cassia fistula plant extract and their photodegradative, antioxidant and antibacterial activities. *Mater. Sci. Semicond. Process.* 31, 446–454. doi: 10.1016/j.mssp.2014.12.023

Travlou, N. A., Ushay, C., Seredych, M., Rodríguez-Castellón, E., and Bandosz, T. J. (2016). Nitrogen-doped activated carbon-based ammonia sensors: effect of specific surface functional groups on carbon electronic properties. *ACS Sens* 1, 591–599. doi: 10.1021/acssensors.6b00093

Umar, M., Ofem, M. I., Anwar, A. S., and Salisu, A. G. (2022). Thermo gravimetric analysis (TGA) of PA6/G and PA6/GNP composites using two processing streams. *J. King Saud Univ. - Eng. Sci.* 34, 77–87. doi: 10.1016/j.jksues.2020.09.003

Voorhis, C., González-Benito, J., and Kramar, A. (2024). Nano in nano"— Incorporation of znO nanoparticles into cellulose acetate-poly(Ethylene oxide) composite nanofibers using solution blow spinning. *Polymers (Basel)* 16, 341. doi: 10.3390/polym16030341

Wang, J., and Guo, X. (2022). Rethinking of the intraparticle diffusion adsorption kinetics model: Interpretation, solving methods and applications. *Chemosphere* 309, 136732. doi: 10.1016/j.chemosphere.2022.136732

Wang, J., Wang, R., Ma, J., and Sun, Y. (2022). Study on the application of shell-activated carbon for the adsorption of dyes and antibiotics. *Water (Basel)* 14, 3752. doi: 10.3390/w14223752

Wong, S., Ghafar, N. A., Ngadi, N., Razmi, F. A., Inuwa, I. M., Mat, R., et al. (2020). Effective removal of anionic textile dyes using adsorbent synthesized from coffee waste. *Sci. Rep.* 10, 2928. doi: 10.1038/s41598-020-60021-6

Xiang, Q., Yu, J., and Wong, P. K. (2011). Quantitative characterization of hydroxyl radicals produced by various photocatalysts. *J. Colloid Interface Sci.* 357, 163–167. doi: 10.1016/j.jcis.2011.01.093

Yadav, M., Singh, N., Annu, Khan, S. A., Raorane, C. J., and Shin, D. K. (2024). Recent advances in utilizing lignocellulosic biomass materials as adsorbents for textile dye removal: A comprehensive review. *Polymers (Basel)* 16, 2417. doi: 10.3390/polym16172417

Yusuf, A., Budiantono, R., Juangsa, F. B., Aziz, M., Budiyanto, M. A., Saputro, A. G., et al. (2025). Insights into the role of metal dopant on ammonia decomposition over graphene-supported Ni6, Ni5Pt, and Ni5Rh clusters. *Int. J. Hydroge Energy* 130, 168–175. doi: 10.1016/j.ijhydene.2025.04.357

Zhang, T., Guan, X., Zhu, B., Zhang, Z., Ye, X., Zeng, W., et al. (2024b). Boosting solar-driven thermal-assisted photocatalytic hydrogen production through device thermal management. *Int. J. Hydroge Energy* 51, 921–934. doi: 10.1016/j.ijhydene.2023.07.103

Zhang, Z., Wang, X., Long, J., Ding, Z., Fu, X., and Fu, X. (2010). H2–O2 promoting effect on photocatalytic degradation of organic pollutants in an aqueous solution without an external H2 supply. *Appl. Catal A Gen.* 380, 178–184. doi: 10.1016/j.apcata.2010.03.057

Zhang, J., Wu, H., Shi, L., Wu, Z., Zhang, S., Wang, S., et al. (2024a). Photocatalysis coupling with membrane technology for sustainable and continuous purification of wastewater. *Sep. Purif. Technol.* 329, 125225. doi: 10.1016/j.seppur.2023.125225

Zhen, X., Fan, C., Tang, L., Luo, J., Zhong, L., Gao, Y., et al. (2023). Advancing charge carriers separation and transformation by nitrogen self-doped hollow nanotubes g-C3N4 for enhancing photocatalytic degradation of organic pollutants. *Chemosphere* 312, 137145. doi: 10.1016/j.chemosphere.2022.137145